

Research

Nonlinear Scattering from Partially Closed Cracks and Imperfect Interfaces

Claudio Pecorari

May 2004

SKI perspective

Background

The project was set up to investigate the potential of nonlinear scattering phenomena as new tools to detect and localize stress-corrosion cracks in components of nuclear power plants. Partial contact between the faces of a crack reduces the linear acoustic contrast such a defect offers when it is completely open, and, thus, it often tends to make the crack transparent to inspecting waves used in conventional methods. However, the two-dimensional distribution of contacts between asperities of the crack surfaces forms a physical system with nonlinear mechanical properties. The latter are determined both by the force law governing the interaction between individual asperities in contact and by the topographical properties of the distribution. Therefore, the generation of nonlinear wave components upon ultrasound scattering becomes a conceivable alternative to linear scattering phenomena to detect partially closed cracks.

Purpose of the project

The main purpose of this project has been the theoretical and experimental investigation of the conditions under which nonlinear scattering of ultrasonic waves by partially closed surface-breaking cracks may occur and be observed.

Results

These results demonstrate the potential offered by nonlinear scattering phenomena as new tools to inspect material components in search of partially closed cracks. They also give clear indications on the design of the experimental set-ups which better realize such potential.

Project information

Responsible for the project at SKI has been Peter Merck.
SKI reference: 14.43-010902/21156

Research

Nonlinear Scattering from Partially Closed Cracks and Imperfect Interfaces

Claudio Pecorari

MWL

Department of Aeronautics and Vehicle Engineering

Royal Institute of Technology

SE-100 44 Stockholm

Sweden

May 2004

This report concerns a study which has been conducted for the Swedish Nuclear Power Inspectorate (SKI). The conclusions and viewpoints presented in the report are those of the author/authors and do not necessarily coincide with those of the SKI.

Table of content

Summary.....	3
Sammanfattning.....	5
1 Introduction	7
2 Theory.....	8
2.1 Introduction	8
2.2 Rough surfaces in contact: elastic case	9
2.2.1 Normal interfacial stiffness	9
2.2.2 Tangential interfacial stiffness	11
2.2.3 Effective nonlinear boundary conditions.....	12
2.2.4 Reflection and transmission of plane waves	13
2.3 Rough surfaces in contact: adhesive interface.....	23
2.3.1 Micromechanics of a single contact	23
2.3.2 Rough surfaces in contact.....	25
2.3.3 Wave reflection and transmission	30
2.3.4 Concluding remarks.....	36
2.4 Scattering by a surface-breaking crack.....	37
2.4.1 Introduction	37
2.4.2 Theory.....	39
2.4.3 Numerical results.....	45
2.4.4 Summary and concluding remarks	54
3 Experimental investigation.....	56
3.1 Introduction	56
3.2 Steel-steel interfaces: experimental results	56
4 Summary and concluding remarks	61
5 Acknowledgments	61
6 References	62

Summary

This project has investigated the potential offered by nonlinear scattering phenomena to detect stress-corrosion, surface-breaking cracks, and regions of extended interfaces which are often invisible to conventional inspection methods because of their partial closure and/or the high background noise generated by the surrounding microstructure.

The investigation has looked into the basic physics of the interaction between ultrasonic waves and rough surfaces in contact, since the latter offers a prototypical example of a mechanical system which is characterized by a dynamics similar to that of a partially closed crack. To this end, three fundamental mechanisms which may be activated by an inspecting ultrasonic wave have been considered. The first mechanism is described by the Hertz force law which governs the interaction between asperities in contact that are subjected to a normal load. The second mechanism considers the dynamics of two spherical asperities subjected to an oscillating tangential load. To this end, the model developed by Mindlin and Deresiewicz (1953) have been used. The third mechanism accounts for the effect of forces of adhesion, and can be described by a model developed by Greenwood and Johnson (1998). The validity of this model is rather general and covers the extreme cases of very soft and very rigid contacts. This model aims at describing the effect of fluid layers with thickness of atomic size, which may be present within a crack.

Statistical models accounting for the topography of the two rough surfaces in contact have been developed, and the macroscopic stiffness of the interface recovered. These results have been used to formulate effective boundary conditions to be enforced at the interface, and the reflection and transmission problem has been solved in a variety of situations of experimental significance.

The main conclusion of this part of the project is that the second harmonic component is the dominant feature of the nonlinear response of an interface formed by two rough surfaces in contact. The amplitude of the second harmonic wave is shown to reach a maximum value when the interface normal stiffness, K_N , is approximately equal to the product of shear acoustic impedance of the material and the wave's angular frequency, ω . For increasing values of K_N the nonlinear response of the interface is shown to slowly decrease.

The boundary conditions for elastic interfaces have been used to investigate the scattering of a two-dimensional surface-breaking crack which is insonified by either a shear-vertical (SV) wave or a Rayleigh wave. A mathematical model describing these phenomena has been developed, and several parametric studies have been carried out. The numerical results indicate that the largest nonlinear response is obtained when an SV wave insonifies the crack at angles of incidence which are just above the critical angle for longitudinal waves. A simple explanation for this finding has been provided in terms of the dependence of the total stress field acting on the plane containing the crack. As already observed for infinite interfaces, even the acoustic response of a partially closed surface-breaking crack shows a sharp rise when the crack begins to close, reaches a maximum value and slowly decreases as the closure of the interface progressively increases.

A series of experiments have been conducted to assess the magnitude of the nonlinear generation of interfaces formed by two rough steel surfaces in contact. Preliminary results show a general qualitative agreement with the theoretical models earlier developed in this project. Above all, the amplitude of the second harmonic component reaches values that are at least 20 dB above the threshold of the noise.

Signals having amplitudes of that order of magnitude have been recorded also for applied pressure values comparable to the largest residual stresses measured in welds. These findings provide a solid ground on which the future development of nonlinear ultrasonic methods for the detection of partially closed cracks embedded into a medium with coarse microstructure can be based.

Sammanfattning

Detta projekt undersöker det icke linjära spridningsfenomenet och dess möjligheter att detektera ytbrytande, spänningskorrosion sprickor. Dessa kan vara osynliga för konventionella metoder då sprickorna delvis eller helt är slutna och/eller att brusnivån från mikrostrukturella effekter överröstar signalen.

Fysikaliska fenomen som beskriver växelverkan mellan ultraljudsvågor och skrovliga ytor i kontakt har undersökts. Detta mekaniska system innehåller liknande dynamik som en partiellt sluten spricka och utgör därför ett bra prototypexempel. Tre olika mekanismer har undersökts. Den första beskrivs av Hertz kraftlag för växelverkan mellan sfäriska skrovligheter i kontakt utsatta för en last i linje med kontaktytans normal. Den andra mekanismen bestämmer dynamiken mellan två sfäriska skrovligheter utsatta för en oscillerande tangentiell kraft. Här har en modell utvecklad av Mindlin och Deresiewicz (1953) använts. Den tredje mekanismen beaktar effekten av krafter som uppkommer vid vidhäftning, vilken kan beskrivas av en modell utvecklad av Greenwood och Jonsson (1998). Giltigheten för denna modell är tämligen generell och omfattar flera situationer från mycket mjuk till rigid kontakt. Denna modell syftar till att beskriva effekten av fluida lager med tjocklekar på atomnivå vilket kan vara fallet i en spricka.

Statistiska modeller som beaktar topologin för de två skrovliga ytorna i kontakt har utvecklats varifrån gränsskiktets makroskopiska styvhet beräknats. Resultaten har använts för att skapa effektiva randvillkor som krav vid ytorna, och reflexion och transmissionsproblemen har lösts för en rad olika fall.

Huvudslutsatsen så här långt är att andra ordningens harmoniska komponent är dominerande för den icke linjära responsen från en gränssyta formad av två skrovliga ytor i kontakt med varandra. Amplituden från andra ordningens harmoniska våg visas nå sitt maximum när gränssytans normaliserade styvhet, K_N , är approximativt lika med produkten av materialets akustiska skjuvimpedans och vågens vinkelfrekvens, ω . För ökande värden på K_N avtar den icke linjära responsen långsamt.

Randvillkoren för elastiska gränssytor har använts för att undersöka spridningen av en två-dimensionell ytbrytande spricka vilken träffas av antingen en vertikal skjuv våg (SV) eller en Rayleigh våg. En matematisk modell som beskriver dessa fenomen har utvecklats, och ett antal parameterstudier har gjorts. De numeriska resultaten indikerar att den största icke linjära respons fås när en SV våg träffar sprickan med en infallsvinkel som är omkring den kritiska vinkeln för longitudinella vågor. En enkel förklaring till detta har åskådliggjorts i termer av det totala spänningsfältet över sprickan och dess avhängighet till infallsvinkeln. Den icke linjära responsen från sprickan ökar när sprickan börjar slutas, når ett maxvärde och avtar långsamt då avståndet mellan gränssytorna progressivt minskar. Detta uppträdande har tidigare visats för infinita gränssytor.

En rad experiment har utförts för att fastställa storleken på den icke linjära genereringen från två skrovliga gränssytor i kontakt. Preliminära resultat visar ett generellt kvalitativt överensstämmande med de teoretiska modeller som utvecklats. Utöver detta, när amplituden av andra ordningens harmoniska komponent värden som är minst 20 dB över brusets tröskelvärde. Signaler med amplituder av dessa storlekar har uppmätts för

ihoptryckta ytor där spänningarna kan jämföras med de högsta residuala spänningsvärden som uppmätts i svetsar. Dessa upptäckter ger en solid grund för vidare utveckling av icke linjära ultraljudsmetoder för detektering av partiellt slutna sprickor i medium med grov mikrostruktur.

1 Introduction

The project “*Nonlinear Scattering from Partially Closed Cracks and Imperfect Interfaces*” was set up to investigate the potential of nonlinear scattering phenomena as new tools to detect and localize stress-corrosion cracks in components of nuclear power plants. The rationale supporting the expectation that such phenomena may appear when stress-corrosion cracks are insonified by an ultrasonic wave relies on the same fact that decreases their probability of detection by means of conventional techniques: under the conditions in which routine inspections are carried out, the faces of a stress-corrosion crack are in partial contact.

Partial contact between the faces of a crack reduces the linear acoustic contrast such a defect offers when it is completely open, and, thus, it tends to make the crack transparent to inspecting waves used in conventional methods. However, the two-dimensional distribution of contacts between asperities of the crack surfaces forms a physical system with *nonlinear mechanical properties*. The latter are determined both by the force law governing the interaction between individual asperities in contact and by the topographical properties of the distribution. Therefore, the generation of nonlinear wave components upon ultrasound scattering becomes a conceivable alternative to linear scattering phenomena to detect partially closed cracks.

The main purpose of this project, therefore, has been the theoretical and experimental investigation of the conditions under which nonlinear scattering of ultrasonic waves by partially closed surface-breaking cracks may occur and be observed.

The report is structured in two main sections. The first one gives an account of the results obtained in the theoretical investigation of this problem. In particular, two models are presented in which the nonlinear mechanical properties of two types of interfaces of infinite extent are modelled. The first model deals with contacts that are purely elastic, while the second one considers contacts which are subjected also to the effect of forces of adhesion. As explained in the text with more details, the motivation behind the second model resides in the fact that stress-corrosion cracks develop in wet environments. The outcome of this part of the study has been the formulation of new effective nonlinear boundary conditions to be enforced at the crack surface. The boundary conditions for purely elastic contacts have been implemented in a new model dealing with the linear and nonlinear scattering of a surface-breaking crack with faces in partial contact. In this work both Rayleigh wave incidence and shear vertical (SV) incidence have been considered.

Finally, the second part of the project reports the experimental results that have been obtained on steel-steel rough interfaces in contact. In particular, the generation of the second harmonic wave is investigated as a function of the interface conditions. It is shown that, depending on the interface properties, second harmonic signals can be measured having amplitude values more than 30 dB above the threshold of the noise. The experimental part of the project could not be developed as planned in the original proposal because of serious difficulties in obtaining the funds necessary to the acquisition of the instrumentation required by this type of work. Therefore, the author is particularly grateful to the Swedish Centre for Nuclear Technologies (SKC) for its

financial support which allowed the purchase of the instrumentation necessary to achieve the results presented next, and for sponsoring a scholarship on the issues dealt with in this project.

The material generated in this project has been published (Pecorari (2003)) or is under review in three publications in the Journal of the Acoustical Society of America (JASA) (Pecorari (2004a), and Pecorari and Poznic (2004b)), and has been presented in six international conferences. Additionally, a fourth one, reporting the preliminary experimental results on the generation of nonlinear waves by imperfect interfaces is in preparation. Also under preparation is a joint contribution with Prof. Igor Solodov of the State University of Moscow to a book entitled *The universality of Nonclassical nonlinearity* which will be published with the support of the European Science Foundation and as a part of the activity of the network NATEMIS. This network offers a forum to European researchers involved with scientific and applied issues related to nonlinear acoustic phenomena in materials with mesoscopic structure and damage.

2 Theory

2.1 Introduction

The first theoretical task tackled in this project has been the derivation of effective boundary conditions which include the nonlinear dynamics of the contacting crack's surfaces. To this end, two micromechanical models have been derived which deal with two physical situations that may plausibly be encountered when dealing with stress corrosion cracks. In the first model the nonlinear macroscopic behaviour emerging from the purely elastic interaction between surface asperities in contact is examined. In the second model, the addition of forces of adhesion is considered in order to model the effect of a thin fluid layer that may be present within the crack. Such an expectation is justified by the fact that stress-corrosion cracks develop in wet environments.

The simplest available framework to treat the problem of wave scattering from imperfect interfaces is the spring model (Baik and Thompson, 1984), an effective medium approach in which the actual interface is substituted by a distribution of springs having no thickness, and stiffness, K , with values ranging between 0 and infinity. For $K = 0$, the materials forming the interface are completely detached from each other and the total stress at their surfaces is null (no bond). For $K = \infty$, a perfect bond is realized between the materials, and the continuity of the displacement field across the interface is satisfied. This approach provides no information regarding the physical nature of the interfacial defects, leaving the problem of linking the spring model to the physics of a specific real system to some additional and independent micromechanical description of the latter. The validity of the spring model is limited to frequencies at which the individual nature of the scatterers is not manifested. As the frequency of the inspecting wave increases, the individual nature of the defects becomes apparent, and the spring model ceases to be valid.

In the following, the above mentioned models and the associate acoustic phenomena which are of some relevance for this investigation are presented.

2.2 Rough surfaces in contact: elastic case

2.2.1 Normal interfacial stiffness

By using Greenwood and Williamson's model (Greenwood and Williamson, 1966), and Hertz analysis of the contact between two elastic spheres (Johnson, 1985), the relationship between the normal pressure, P , and the relative approach, δ , between the mean planes of the contacting surfaces is found to be (Greenwood and Williamson, 1966, Brown and Scholz, 1985, Baltazar *et al.* 2002)

$$P = \frac{2}{3} n \left\langle \frac{E}{1-\nu^2} \right\rangle \langle R^{1/2} \rangle \int_0^{\delta} (\delta - z)^{3/2} \varphi(z; N) dz, \quad (1)$$

In this approach, the load-bearing asperities are assumed to be independent of each other, limiting the validity of the model to those situations in which only a small fraction of the total number of asperities are in contact. From eq. (1), Baltazar *et al.* (2002) derived the following expression for the normal interface stiffness, K_N ,

$$K_N = \frac{\partial P}{\partial \delta} = n \left\langle \frac{E}{1-\nu^2} \right\rangle \langle R^{1/2} \rangle \int_0^{\delta} (\delta - z)^{1/2} \varphi(z; N) dz. \quad (2)$$

In eq. (1) and (2), φ is the height distribution of the asperities of the composite surface (Fig. 1). The latter is defined by an appropriate algebraic combination of the profiles of the two rough surfaces of interest, which maps the individual contacts between the asperities of the two surfaces into the peaks of the composite one. The variable z is defined by the transformation $z = Z_o - z'$, where Z_o is the coordinate of the highest asperities of the composite surface, and z' is the actual coordinate of the asperity measured from the surface mean plane. Thus, $\varphi(z)dz$, which gives the number of peaks with height between z and $z + dz$ above the mean plane of the composite surface, that is to say, the number of contacts formed in this interval. Note that $\varphi(z) = 0$ for $z' > Z_o$. n is the number of contacts per unit area, E and ν are the Young modulus and the Poisson ratio of the material, respectively, and R is the radius of curvature of the asperities.

Following Adler and Firman (1981), and Brown and Scholz (1985), this function is properly modelled by an inverted chi-squared distribution that depends on an integer parameter, $N \geq 2$, known as the 'number of degrees of freedom' (see also Baltazar *et al.* 2002),

$$\varphi(z; N) = \left(\sqrt{\frac{2}{N}} \Sigma \right)^{-\frac{N}{2}} \frac{(z)^{(N-2)/2}}{\Gamma(N/2)} \exp\left(-\sqrt{\frac{N}{2}} \frac{z}{\Sigma} \right). \quad (3)$$

The symbol $\Sigma = (\sigma_1^2 + \sigma_2^2)^{1/2}$ represents the rms roughness of the composite interface, while σ_1 and σ_2 are those of the individual surfaces. For $N = 2$, $\varphi(z, N)$ is an exponential function with an absolute maximum at $z = 0$, while it approaches a Gaussian distribution as N increases. This choice for $\varphi(z; N)$ provides the required flexibility to model the topographical properties of the two surfaces. The nonlinear nature of the

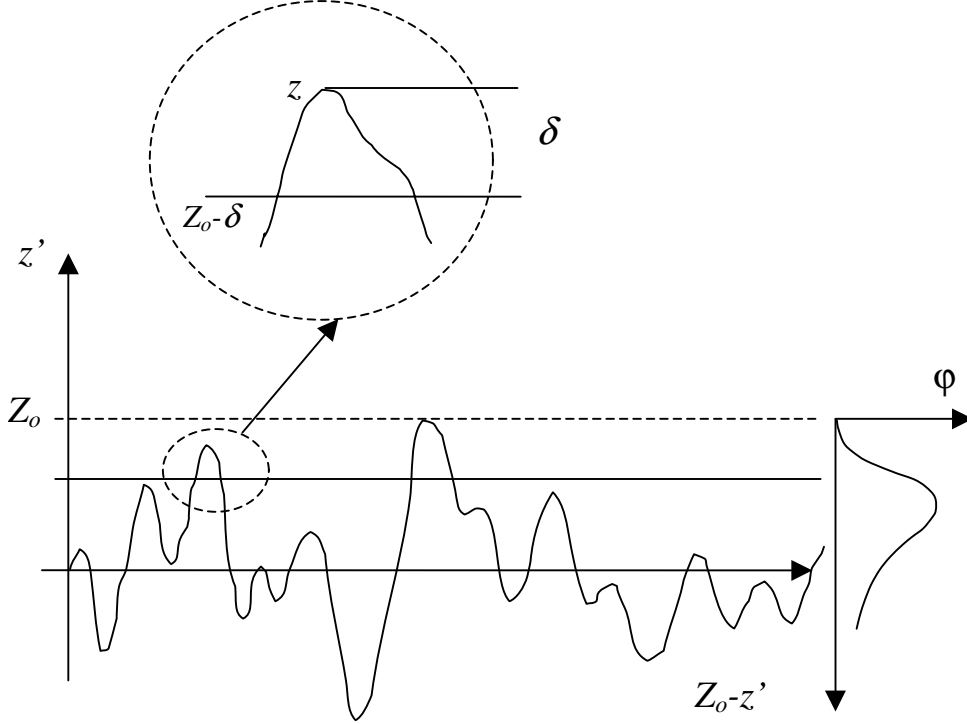


Figure 1. Coordinates systems for the profile of the composite surface and for the probability density function of its asperities. The inset explains the relation between the coordinate of the flat rigid surface pressed against the composite one, the deformation of a given asperity, and the coordinates of the profile.

dependence of K_N can be accounted for by considering the expansion of K_N in powers of $\Delta\delta$ in which the first order term is retained,

$$K_N(\delta + \Delta\delta) = K_N(\delta) + \frac{\partial K_N}{\partial \delta} \Delta\delta = K_{N,0} + K_{N,1} \Delta\delta. \quad (4)$$

In eq. (4), the constant $K_{N,0}(\delta)$ can be evaluated by means of eq. (2), while $K_{N,1}$ is given by

$$K_{N,1} = \frac{\partial K_{N,0}}{\partial \delta} = \frac{n}{2} \left\langle \frac{E}{1-\nu^2} \right\rangle \langle R^{1/2} \rangle \int_0^\delta (\delta - z)^{-1/2} \varphi(z; N) dz, \quad (5)$$

The variation of the relative approach $\Delta\delta$ is positive when the distance between the mean planes of the two surfaces decreases. Using eq. (5), it can be shown that $K_{N,1}$, although more slowly than $K_{N,0}$, tends to zero for vanishing values of δ , i.e., when the contacts are removed.

2.2.2 Tangential interfacial stiffness

Mindlin and Deresiewicz (1953) derived the relationship between an oscillating tangential force, F_{tan} , and the relative tangential displacement, Δu , of two spheres that are maintained in contact by a normal load, L . Their result, recast in a form suitable for the present work, is

$$F_{tan} = \frac{4}{3} \frac{E}{1-\nu^2} R^{1/2} \delta^{3/2} f \operatorname{sgn}\left(\frac{\partial \Delta u}{\partial t}\right) \left\{ 1 - \left[1 - \frac{1-\nu}{2-\nu} \frac{1}{\delta f} \left(\Delta u_{max} + \operatorname{sgn}\left(\frac{\partial \Delta u}{\partial t}\right) \Delta u \right) \right]^{3/2} - \frac{1}{2} \left[1 - \left(1 - \frac{2(1-\nu)}{2-\nu} \frac{\Delta u_{max}}{\delta f} \right)^{3/2} \right] \right\}, \quad (6)$$

where, as before, δ is the relative approach caused by the normal load applied to the two surfaces, f is the material static coefficient of friction, and Δu_{max} is the maximum, positive tangential displacement reached during a cycle. The function $\operatorname{sgn}(\cdot)$ is equal to 1 when its argument is positive, and to -1 when it is negative. Equation (6) describes a hysteretic loop, the origin of which rests in the relative partial slipping of the contacting spheres. Such a relative displacement occurs within an annulus that extends from the edge of the contact area towards its centre as the strength of the tangential force, F_{tan} , increases. The two spheres undergo complete sliding when $F_{tan} = f L$. For small tangential displacements, eq. (6) can be approximated by

$$F_{tan} \cong \frac{2E}{(1+\nu)(2-\nu)} R^{1/2} \delta^{1/2} \Delta u - \frac{2E(1-\nu)}{(1+\nu)(2-\nu)^2} \frac{1}{f} \left(\frac{R}{\delta}\right)^{1/2} \left[(\Delta u^2 - \Delta u_{max}^2) \operatorname{sgn}\left(\frac{\partial \Delta u}{\partial t}\right) + \Delta u \Delta u_{max} \right]. \quad (7)$$

To account for the effect of a possible modulation of the normal load, eq. (7) can be further generalized by including a term that is proportional to the product of $\Delta \delta \Delta u$,

$$F_{tan} \cong \frac{2E}{(1+\nu)(2-\nu)} R^{1/2} \delta^{1/2} \Delta u + \frac{E}{(1+\nu)(2-\nu)} \left(\frac{R}{\delta}\right)^{1/2} \Delta \delta \Delta u - \frac{2E(1-\nu)}{(1+\nu)(2-\nu)^2} \frac{1}{f} \left(\frac{R}{\delta}\right)^{1/2} \left[(\Delta u^2 - \Delta u_{max}^2) \operatorname{sgn}\left(\frac{\partial \Delta u}{\partial t}\right) + \Delta u \Delta u_{max} \right]. \quad (8)$$

Within the framework of the Greenwood and Williamson approach, eq. (8) can be extended to the whole interface,

$$\Sigma = K_{T,0}\Delta u + K_{T,N}\Delta u\Delta\delta - \frac{1}{2}K_{T,1}\left[(\Delta u^2 - \Delta u_{\max}^2)\text{sgn}\left(\frac{\partial\Delta u}{\partial t}\right) + \Delta u\Delta u_{\max}\right], \quad (9)$$

where Σ is the shear stress acting on the interface, and $K_{T,0}$, $K_{T,N}$, and $K_{T,1}$ are defined by

$$K_{T,0} = 2n\left\langle\frac{E}{(1+\nu)(2-\nu)}\right\rangle\left\langle R^{1/2}\right\rangle\int_0^\delta(\delta-z)^{1/2}\varphi(z)dz, \quad (10)$$

$$K_{T,N} = n\left\langle\frac{E}{(1+\nu)(2-\nu)}\right\rangle\left\langle R^{1/2}\right\rangle\int_0^\delta(\delta-z)^{-1/2}\varphi(z)dz, \quad (11)$$

$$K_{T,1} = 2n\left\langle\frac{E(1-\nu)}{(1+\nu)(2-\nu)^2}\right\rangle\frac{\langle R^{1/2}\rangle}{\langle f\rangle}\int_0^\delta(\delta-z)^{-1/2}\varphi(z)dz, \quad (12)$$

respectively. A comparison between eq. (5), (11) and (12) shows that $K_{T,N}$, and $K_{T,1}$ are proportional to $K_{N,1}$. In addition, the expression found for $K_{T,0}$ is found to be identical to that given by Baltazar *et al.* (2002), and, as discussed in that work, requires a correction factor ξ of the order of 0.5. A correction to eq. (10) is necessary to account for the effect of the angle of misalignment between the centres of the spherical contacts with respect to the line of action of the normal load. Henceforth, such a factor will be included in the definition of the above coefficients.

2.2.3 Effective nonlinear boundary conditions

In this section, the boundary conditions to be enforced at a nonlinear interface between two rough surfaces in elastic contact are formulated. They are

$$\sigma_{31}^+ = K_{T,0}\Delta u - K_{T,N}\Delta v\Delta u - \frac{1}{2}K_{T,1}\left[(\Delta u^2 - \Delta u_{\max}^2)\text{sgn}\left(\frac{\partial\Delta u}{\partial t}\right) + \Delta u\Delta u_{\max}\right] \quad (13.a)$$

$$\sigma_{33}^+ = K_{N,0}\Delta v - K_{N,1}\Delta v^2, \quad (13.b)$$

$$\sigma_{31}^+ = \sigma_{31}^- \quad (13.c)$$

$$\sigma_{33}^+ = \sigma_{33}^-, \quad (13.d)$$

In eq. (13), the superscripts ‘+’ and ‘-’ refer to the positive and negative sides of the interface, and the subscripts 1 and 3 identify the direction parallel and normal to the interface, respectively. Similarly, u and v are the displacement components parallel and normal to the interface, respectively. The latter is assumed to lie in the plane of equation $x_3 = 0$. Eq. (13.a) is derived from eq. (9) by identifying the variation of the relative approach, $\Delta\delta$, with $-\Delta v$, i.e., the out-of-plane displacement discontinuity at the interface. This equation accounts for the hysteretic behaviour of the interface when it is subjected to a shear stress. Eq. (13.b) describes the behaviour of an interface that softens as it opens. The stress fields are continuous at the interface. In eq. (13.a-d), all the field quantities must be understood to be functions of the position along the x -axis, and of time, t .

2.2.4 Reflection and transmission of plane waves

In the following, the boundary value problem posed by eq. (13.a-d) is solved for an incident plane having an arbitrary angle of incidence and polarization. To this end, a simple perturbation approach is used which exploits the harmonic balance method.

2.2.4.1 Longitudinal wave at normal incidence

Let $v_{in}(x_3, t) = A_{in} \hat{x}_3 \exp[j(\omega t - k_L x_3)]$ be the incident longitudinal wave of angular frequency ω and wavenumber $k_L = \omega / C_L$, where C_L is the phase velocity of the wave. Let $v^-(x_3, t)$ and $v^+(x_3, t)$ be the total displacement fields in the negative ($x_3 < 0$) and positive ($x_3 > 0$) half-space, respectively. By introducing these field variables in eq. (13), and by using appropriate normalization constants, the boundary conditions for this problem become

$$\frac{\partial V^+}{\partial X_3} = \frac{\bar{K}_{N,0}}{\kappa^2} (\Delta V - \varepsilon_N \Delta V^2) , \quad (14.a)$$

$$\frac{\partial V^+}{\partial X_3} = \frac{\partial V^-}{\partial X_3} , \quad (14.b)$$

In eq. (14), $v^{+,-} = A_{in} V^{+,-}$, $\Delta V = V^+ - V^-$, $\kappa = C_L / C_T$, where C_T is the shear phase velocity, $x_3 = X_3 / k_T$, where $k_T = \omega / C_T$ is the shear wavenumber, $\bar{K}_{N,0} = K_{N,0} / Z_T \omega$, where Z_T is the shear acoustic impedance of the medium, and, finally, $\varepsilon_N = A_{in} K_{N,1} / K_{N,0}$. Furthermore, a new normalized time variable, τ , is introduced, which is defined by $\tau = \omega t$. Note that the coefficient ε_N does not represent an intrinsic property of the interface. Rather, it measures the variation of the interfacial stiffness caused by a variation of the relative approach, δ , equal to the amplitude of the incident wave, A_{in} . Figure 2 shows plots of ε_N versus the normalized interfacial stiffness $\bar{K}_{N,0}$ for two steel interfaces characterized by the parameters of Table 1, where the parameter $M = \frac{2}{3} n \langle E / (1 - \nu^2) \rangle \langle R^{1/2} \rangle$. Of the parameters in Table 1, those that are related to the

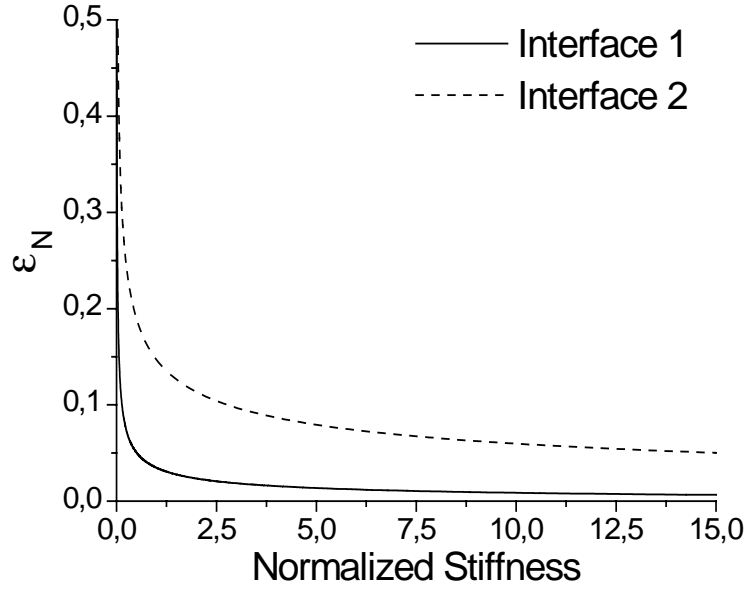


Figure 2. Dependence of the parameter ε_N on the normalized interfacial stiffness for the two interfaces characterized by the parameter of Table 1.

	Roughness (μm)	M ($\text{GPa}/(\mu\text{m}^{3/2})$)	Degrees of Freedom
Interface 1	0.68	5.4	3
Interface 2	0.23	76.8	5

Table 1. Statistical parameters of the interfaces (adapted from Baltazar *et al.* (2002))

interface geometry are obtained from Baltazar *et al.* (2002), while those relating to the material properties have been adapted from the same reference to the case of interest here. The parameters reported by Baltazar *et al.* (2002) were obtained by either direct measurements or best fitting experimental results. Therefore, they can be considered as realistic. The quantity ε_N is evaluated assuming the amplitude and frequency of the incident wave to be $A_{in} = 3$ nm, and 1 MHz, respectively. Thus, the strain produced by this wave is of the order of $3 \cdot 10^{-6}$. Except for a very small region near the origin within which the interface is essentially open, the parameter ε_N is always much smaller than unity. Furthermore, the coefficient ε_N increases as the roughness of the surfaces in contact decreases.

The solution of this problem is searched in terms of a series expansion of the displacement components in the small parameter ε_N :

$$V^{+,-}(\tau) = \sum_{m=0}^{\infty} \varepsilon_N^m V_m^{+,-}(\tau). \quad (15)$$

Introducing eq. (15) into the boundary conditions of eq. (14), and collecting terms according to their expansion order, m , the following systems of boundary conditions are obtained for the zero-th and first order solutions, respectively:

$$\frac{\partial V_0^+}{\partial X_3} - \frac{\bar{K}_{N,0}}{\kappa^2} \Delta V_0 = 0 \quad , \quad (16.a)$$

$$\frac{\partial V_0^+}{\partial X_3} = \frac{\partial V_0^-}{\partial X_3} \quad , \quad (16.b)$$

and

$$\frac{\partial V_1^+}{\partial X_3} - \frac{\bar{K}_{N,0}}{\kappa^2} \Delta V_1 = -\frac{\bar{K}_{N,0}}{\kappa^2} \Delta V_0^2 \quad , \quad (17.a)$$

$$\frac{\partial V_1^+}{\partial X_3} = \frac{\partial V_1^-}{\partial X_3} \quad . \quad (17.b)$$

The solutions of the zero-th order system are waves with the same angular frequency as the incident wave, and complex amplitudes that are proportional to the complex reflection and transmission coefficients for an imperfect interface (Baik and Thompson, 1984),

$$R = -\frac{1}{1 - j2\bar{K}_{N,0}/\kappa} \quad , \quad T = -\frac{j2\bar{K}_{N,0}/\kappa}{1 - j2\bar{K}_{N,0}/\kappa} \quad . \quad (18)$$

The solutions of eq. (17) are determined by the square of the displacement discontinuity between the zero-th order solutions. The latter can be written as a linear combination of a term that is time-independent and describes an increase of the interface opening, and a second one that is proportional to $\exp(j2\tau)$, i.e., it contains the second harmonic of the incident wave. The complex amplitude of the reflected and transmitted second harmonic can be shown to be equal, and are given by

$$A(2\omega) = \varepsilon_N V_1^{+,-} = -\frac{\varepsilon_N}{4} \frac{j\frac{\bar{K}_{N,0}}{\kappa}}{1 - j\frac{\bar{K}_{N,0}}{\kappa}} (T - 1 + R)^2 \quad . \quad (19)$$

According to eq. (18), $A(2\omega)$ is a linear function of A_m through ε_N . Therefore, the amplitude of the physical solution is proportional to the square of the amplitude of the incident wave, A_m^2 . Figure 3 illustrates the dependence of the second harmonic amplitude, $A(2\omega)$, on the normalized interfacial stiffness. As expected, after reaching a

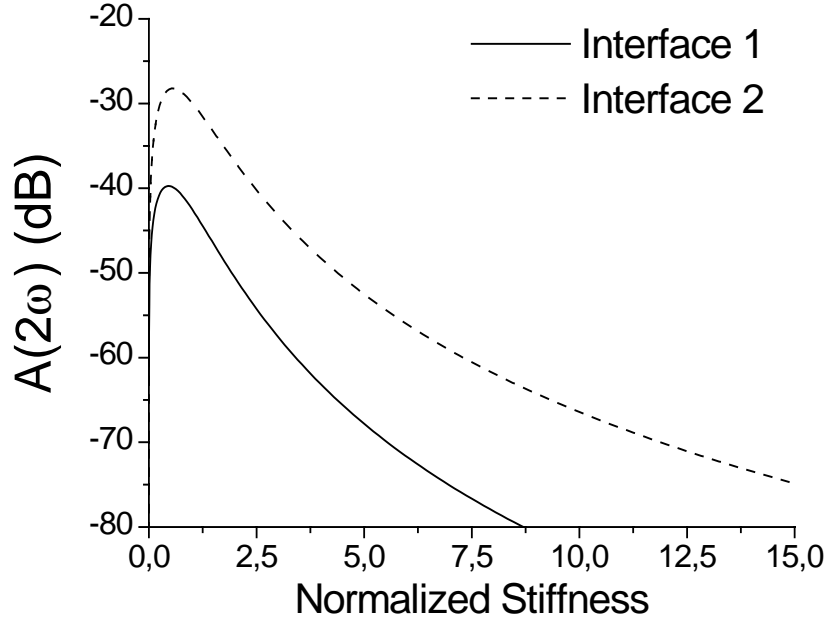


Figure 3. Amplitude of the second harmonic components, $A(2\omega)$, versus the normalized interfacial stiffness for the two interfaces characterized by the parameter of Table 1.

maximum value in the neighbourhood of $\bar{K}_{N,0} = 1$, the nonlinear response of the interface is drastically reduced as the interface becomes stiffer. For the interface with smaller roughness, $A(2\omega)$ reaches values that are only 30 dB below that of the incident wave. Finally, since $\bar{K}_{N,0}$ can be viewed as a function of either R or T , eq. (19) shows that $A(2\omega)$ is the only additional quantity that must be determined experimentally in order to estimate the parameter ε_N .

The next higher-order components in eq. (15) can be shown to contain terms that depend on ω and 3ω , and, thus, do not affect the amplitude of the second harmonic. Therefore, the results of Figure 3 are valid up to the third order in ε_N .

2.2.4.2 Shear wave at normal incidence

A shear wave at normal incidence is considered next. The incident wave is given by $u_{in}(x_3, t) = -A_{in} \hat{x}_1 \exp[j(\omega t - k_T x_3)]$. As in the previous case, sample results are obtained for $A_{in} = 3$ nm, and $\omega = 2\pi$ MHz x rad. The boundary conditions enforced at the interface are

$$\frac{\partial U^+}{\partial X_3} = \bar{K}_T \left[\Delta U - \frac{\varepsilon_T}{2} \left[\text{sgn} \left(\frac{\partial \Delta U}{\partial \tau} \right) (\Delta U^2 - \Delta U_{\max}^2) + \Delta U \Delta U_{\max} \right] \right], \quad (20.a)$$

$$\frac{\partial U^+}{\partial X_3} = \frac{\partial U^-}{\partial X_3}. \quad (20.b)$$

To obtain eq. (20.a, b) from eq. (13.b, d), the normalization constants used in the previous case have been employed. Here again, the perturbation parameter $\varepsilon_T = A_{in} K_{T,1}/K_{T,0}$ can be shown to be much smaller than unity, and, more precisely, smaller than ε_N by a factor of the order of $\frac{1}{f} \frac{1-\nu}{2-\nu}$, which, for steel, is roughly equal to

0.7. Given such a link between ε_N and ε_T , the dependence of ε_T on the interface condition is shown to closely resemble that in Fig. 2, apart from a proper scaling factor of the vertical coordinates. The nonlinear term proportional to the product $\Delta u \Delta v$ is not present in this problem.

The solution is sought by using again the same perturbation expansion as in eq. (15), which leads to the following boundary conditions for the zero-th and first order solutions:

$$\frac{\partial U_0^+}{\partial X_3} - \bar{K}_{T,0} \Delta U_0 = 0 \quad , \quad (21.a)$$

$$\frac{\partial U_0^+}{\partial X_3} = \frac{\partial U_0^-}{\partial X_3} \quad , \quad (21.b)$$

for the zero-th order, and

$$\frac{\partial U_1^+}{\partial X_3} - \bar{K}_{T,0} \Delta U_1 = \frac{\bar{K}_{T,0}}{2} \left[\text{sgn} \left(\frac{\partial \Delta U_0}{\partial \tau} \right) (\Delta U_0^2 - \Delta U_{0,max}^2) + \Delta U_0 \Delta U_{0,max} \right] \quad , \quad (22.a)$$

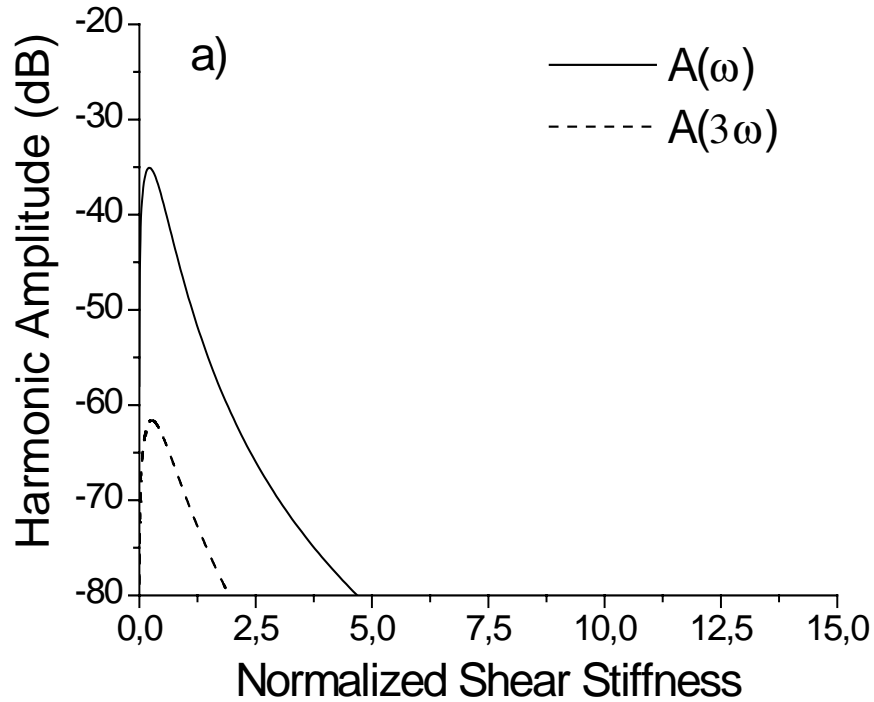
$$\frac{\partial U_1^+}{\partial X_3} = \frac{\partial U_1^-}{\partial X_3} \quad , \quad (22.b)$$

for the first order. In order to obtain eq. (22.a) from eq. (20.a), the function $\text{sgn}(\partial \Delta U / \partial \tau)$ has been approximated by $\text{sgn}(\partial \Delta U_0 / \partial \tau)$ on the ground that the first order solutions are much smaller than those of the zero-th order.

The solutions of the zero-th order system are obtained from those of the previous case (see eq. (18)) by replacing $\bar{K}_{N,0}/\kappa$ with $\bar{K}_{T,0}$. With these terms, the right-hand side of eq. (22.b) can be evaluated, and its time dependence examined in terms of its harmonic content. Expanded in a Fourier series, this source function is shown to be odd with respect to time. Therefore, no even harmonic of the incident wave is generated upon reflection and transmission of a shear wave at normal incidence. A similar result was found by O'Neil *et al.* (2001) for an interface formed by two surfaces coupled by friction. The amplitudes of the odd harmonic waves generated by the nonlinear response of the interface are found by introducing the Fourier representation of the source function on the right-hand side of eq. (22.b) and by solving the partial linear problems into which the original one can be decomposed. The amplitudes are

$$A(n\omega) = -j\varepsilon_T \frac{2\bar{K}_{T,0}}{n - j2\bar{K}_{T,0}} C_n, \quad n = 1, 3, 5, \dots \quad (23)$$

where C_n is the n -th complex coefficient of the Fourier series of the source function. Figure 4 presents plots of the first and higher harmonics generated by the interfaces of Table 1. The third harmonic generated by the interface having a r.m.s. roughness of $0.68 \mu\text{m}$ is more than 60 dB below the amplitude of the incident wave, while that generated by the interface with the smaller roughness reaches -50 dB. The reduced nonlinear response of this kind of interface to a shear excitation, compared to the response to longitudinal wave, can be partly explained by the higher order nonlinearity at which the effect appears, and partly by the magnitude of the coefficient ε_T compared to ε_N . These results indicate that the magnitude of the nonlinear response of interfaces formed by rough surfaces in contact to a longitudinal wave exceeds that to a shear wave by about 20 dB.



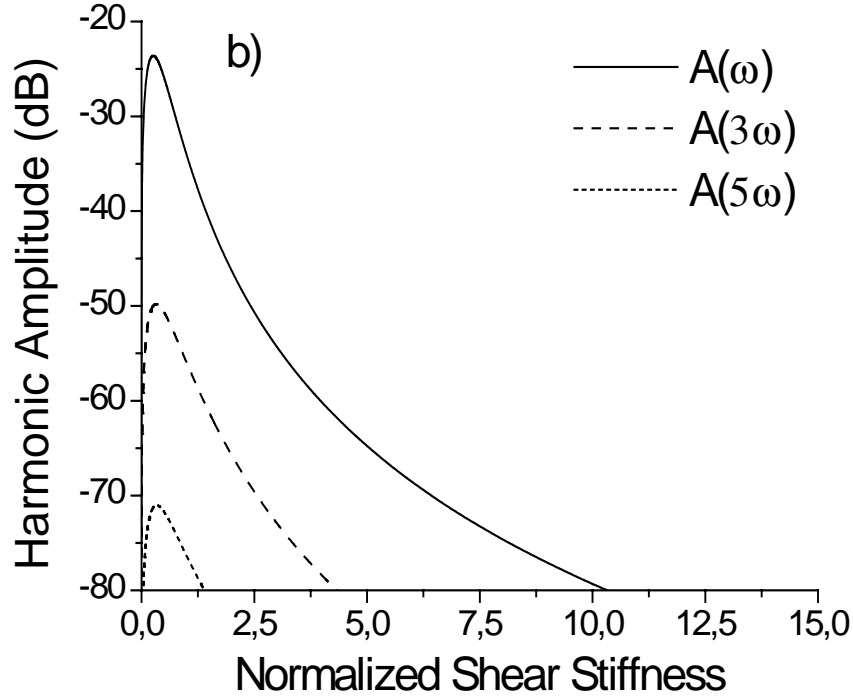


Figure 4. Amplitude of the first three odd harmonic components, $A(n\omega)$, $n = 1, 3, 5$, versus the normalized interfacial shear stiffness for the two interfaces characterized by the parameter of Table 1: a) Interface 1, b) Interface 2.

2.2.4.3 Oblique incidence

In this section, the cases of both longitudinal and shear oblique incidence are considered. For both problems, the boundary conditions for the normalized displacement fields are

$$\frac{\partial V^+}{\partial X_3} + \frac{\partial U^+}{\partial X_1} = \bar{K}_T \left[\Delta V - \varepsilon_N \Delta U \Delta V - \frac{\varepsilon_T}{2} \left[\operatorname{sgn} \left(\frac{\partial \Delta V}{\partial \tau} \right) (\Delta V^2 - \Delta V_{\max}^2) + \Delta V \Delta V_{\max} \right] \right], \quad (24.a)$$

$$\kappa^2 \frac{\partial V^+}{\partial X_3} + (\kappa^2 - 2) \frac{\partial U^+}{\partial X_1} = \bar{K}_{N,0} (\Delta V - \varepsilon_N \Delta V^2), \quad (24.b)$$

$$\frac{\partial V^+}{\partial X_3} + \frac{\partial U^+}{\partial X_1} = \frac{\partial V^-}{\partial X_3} + \frac{\partial U^-}{\partial X_1}, \quad (24.c)$$

$$\kappa^2 \frac{\partial V^+}{\partial X_3} + (\kappa^2 - 2) \frac{\partial U^+}{\partial X_1} = \kappa^2 \frac{\partial V^-}{\partial X_3} + (\kappa^2 - 2) \frac{\partial U^-}{\partial X_1}. \quad (24.d)$$

A comparison between eq. (13.a) and eq. (24.a) shows that, upon normalization, the coefficient K_{NT} leads to ε_N , reducing the number of parameters required to describe

the nonlinearities of the interface to two. The solution of the problem is sought by expanding the displacement field components on both sides of the interface in a double series in the small parameters ε_N and ε_T ,

$$U^{+,-} = U_0^{+,-} + \varepsilon_N U_{1,N}^{+,-} + \varepsilon_T U_{1,T}^{+,-} + O(\varepsilon_N, \varepsilon_T), \quad (25.a)$$

$$V^{+,-} = V_0^{+,-} + \varepsilon_N V_{1,N}^{+,-} + \varepsilon_T V_{1,T}^{+,-} + O(\varepsilon_N, \varepsilon_T). \quad (25.b)$$

Following the perturbation procedure previously employed, the reflected and transmitted waves can be easily found, though they cannot be given by simple analytical expression.

Figure 5 illustrates the first order, nonlinear response of the interface with r.m.s. roughness equal to $0.23 \mu\text{m}$ (see Table 1) as a function of the angle of incidence. The incident wave is longitudinally polarized. Figure 5.a refers to the longitudinal second harmonic component, while Fig. 5.b to the shear second harmonic wave. Similar to the results at normal incidence, the amplitude is shown to initially increase, and rapidly fall as the normalized normal stiffness, \bar{K}_N , becomes greater than 1. Of interest is the relatively small variation of the amplitude of the second harmonic longitudinal wave with the angle of incidence, in view of which the angular dependence of the nonlinear response of a partially closed crack may be expected to resemble that of the linear response. As for the second harmonic shear wave (Fig. (5.b)), its amplitude remains below that of the longitudinal component for all the values of the angle of incidence. The same observation can be made for the amplitude of the third harmonics generated by the hysteretic behaviour of the interface, which, therefore, seems not to play a relevant role.

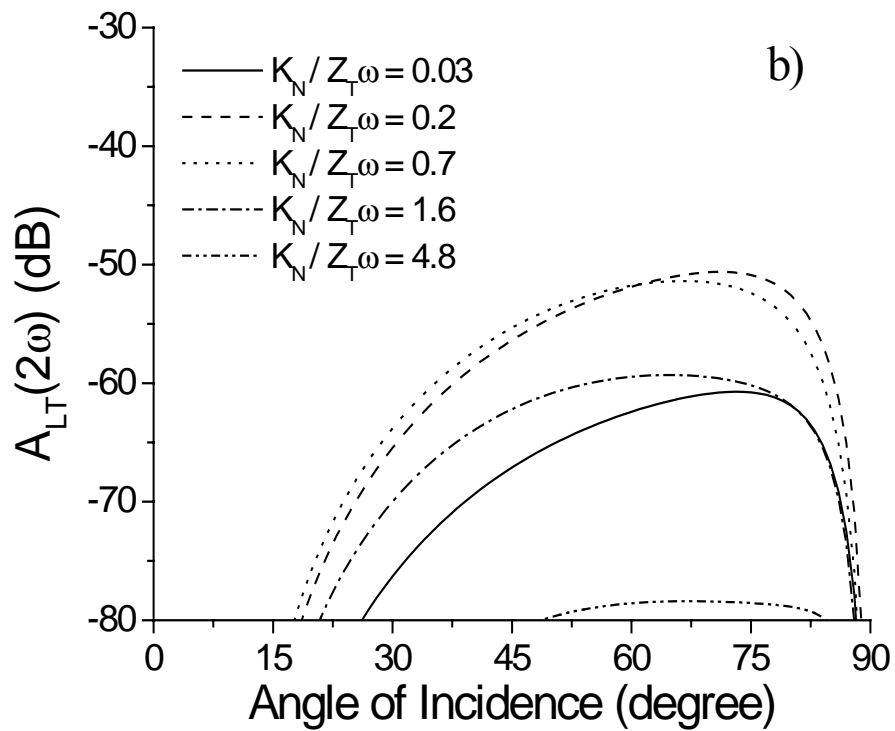
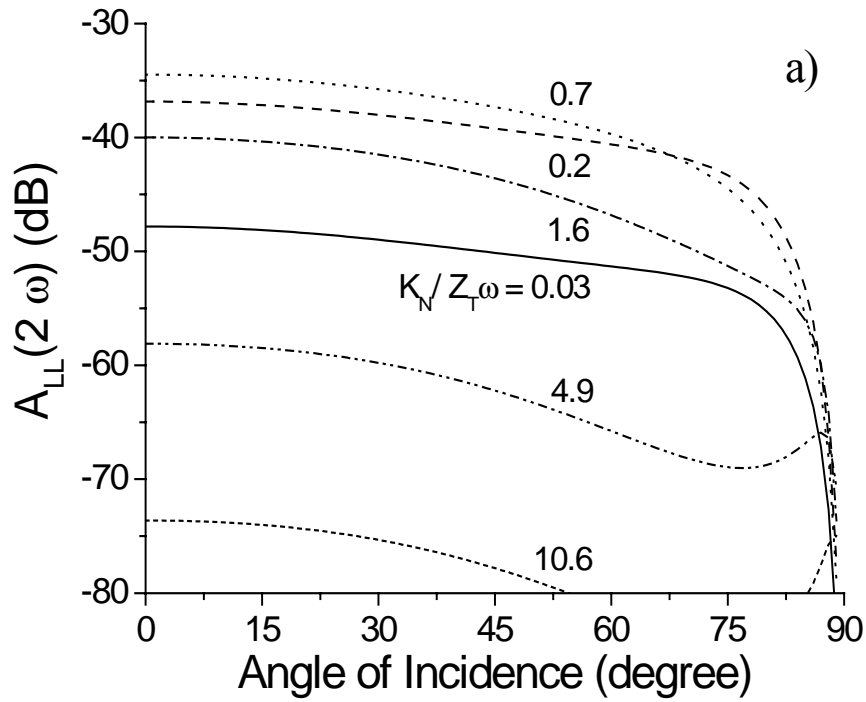


Figure 5. Longitudinal a) and shear b) second harmonic amplitude versus angle of incidence generated upon scattering of a longitudinal incident wave for various values of the normalized normal stiffness.

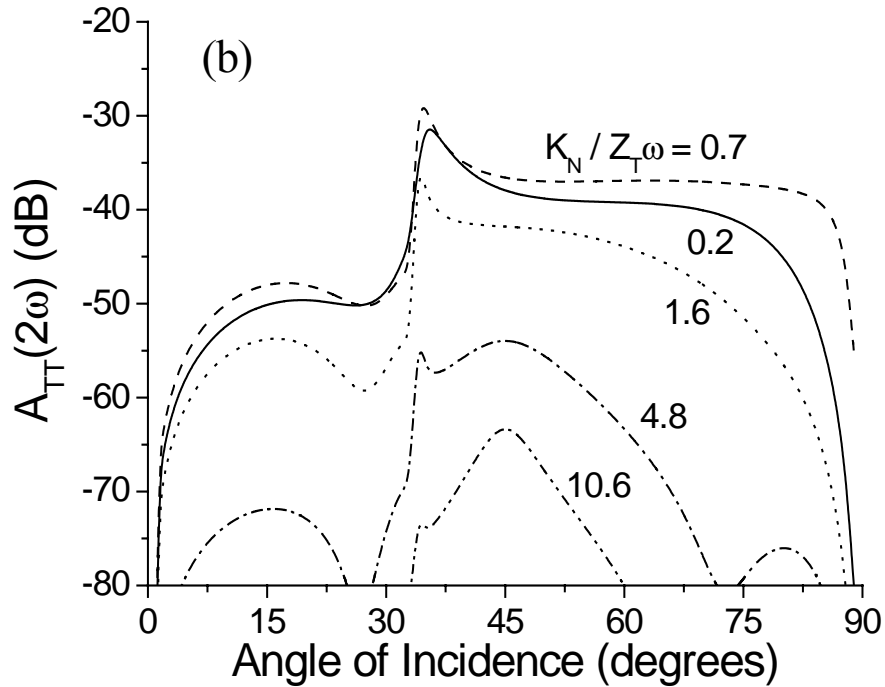
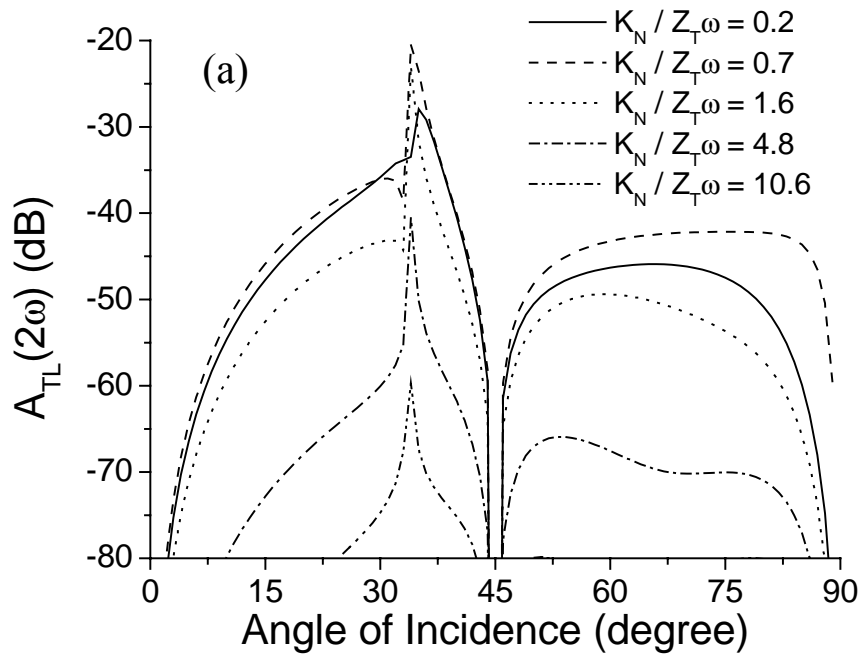


Figure 6. Longitudinal a) and shear b) second harmonic amplitude versus angle of incidence generated upon scattering of a shear incident wave for various values of the normalized normal stiffness.

Figure 6 presents sample results for a shear incident wave. They illustrate the remarkable feature of the amplitude of the longitudinal second harmonic in the neighbourhood of the longitudinal critical angle, which approaches the -20 dB level below the amplitude on the incident wave (Fig. (6a)). Such a result can be explained by the localization of the energy carried by the longitudinal waves in proximity of the interface occurring for values of the angle of incidence near the longitudinal critical angle. Although above the longitudinal critical angle the nonlinear scattered waves may not be used for detection purposes since they do not propagate away from the interface, this result suggests an efficient way to inject energy into the interface in order to enhance its nonlinear response to a second inspecting wave. The shear second harmonic wave (Fig. (6.b)), on the other hand, maintains its propagating character over the whole range of angles of incidence. A similar phenomenon was previously predicted for a perfect interface between two nonlinear materials by Shui *et al.* (1987).

2.3 Rough surfaces in contact: adhesive interface

In the following, a micromechanical model developed by Greenwood and Johnson (1998) (GJ model) to describe the contact between two spherical bodies interacting via both elastic forces and forces of adhesion is presented first. Next, the micromechanics of interacting asperities predicted by the GJ model is incorporated into the framework developed by Greenwood and Williamson (1966) to derive the mechanics of two nominally flat, nonconforming rough surfaces in contact. The case of an interface subjected to a cyclic load is examined in detail. Adhesion between the surfaces in contact is shown to lead to hysteresis with end-point memory in the relationship between the applied stress and the relative approach of the two surfaces. The results of this section are then used to formulate effective boundary conditions to be enforced on the acoustic field of a longitudinal wave at normal incidence. This boundary value problem is finally solved by means of a classical perturbation approach in which two small parameters measuring the nonlinearity of the interface are used as perturbation parameters. The amplitude of higher harmonics is shown to display the features that have previously found in materials with distributed damage and in geomaterials (Guyer and Johnson (1999), Ostrovsky and Johnson (2001), TenCate *et al.* (1996), Meegan *et al.* (1992)). A series of critical remarks on the present work concludes this communication.

2.3.1 Micromechanics of a single contact

The interaction between two spheres, or a sphere and a flat surface, involving both elastic and adhesive forces is controlled by a single parameter, μ , known as the Tabor parameter. In this work, the definition of μ given by Greenwood and Johnson (1998) is adopted: $\mu = \sigma_o \left(R / (E'^2 \Delta\gamma) \right)^{1/3}$ (Note 1). The symbol σ_o is the maximum adhesive stress acting on the contact, R is the composite radius of curvature, which is defined by $R = (R_1^{-1} + R_2^{-1})^{-1}$, where R_1 and R_2 are the radii of curvature of the two spheres, E' is the reduced Young modulus of the contact, $E' = \left((1 - \nu_1^2) / E_1 + (1 - \nu_2^2) / E_2 \right)^{-1}$, and $\Delta\gamma$ is the surface energy. The symbols E_i and ν_i , with $i = 1, 2$, are the Young and the Poisson moduli of the two materials, respectively.

In the GJ model, the interaction between the two bodies in contact is described by superimposing two Hertzian stress distributions of opposite sign. The compressive Hertzian stress, as in the original model by Hertz, acts over a circular area of radius a . The tensile stress, which simulates the effect of adhesion, acts also over a surrounding circular annulus with external radius $c > a$. The Hertzian character of the two distributions allows their superposition to yield a uniform displacement of the points in contact over the area $r < a$. Therefore, like in the original theory by Hertz, the force applied to the centers of the spheres, $F = F(\delta | \mu)$ (Note 2), can be related to the relative approach of such points, δ . However, no simple direct mathematical relationship exists between the two quantities. Rather, four equations are given to link δ and F , which involve four additional model parameters: a , c , μ , and k . The latter parameter, which controls the intensity of the tensile stress, is introduced in the model to obtain a uniform displacement distribution of points for which $r < a$.

By varying the Tabor parameter between 0 and ∞ , the whole spectrum of cases ranging from that of two rigid spheres in contact (Bradley (1932), $\mu = 0$) to that contemplated by Johnson, Kendall and Roberts (1971) (the JKR model, $\mu \rightarrow \infty$) can be covered. The latter properly describes the case of a contact characterized by large values of R and surface energy, and/or between rather soft materials. For a thorough discussion and rigorous analysis of the interaction of two spheres the reader is referred to the work of Greenwood (1998).

Fuller and Tabor (1975) described the adhesion between nominally flat, rough surfaces of Perspex and rubber by implementing the JKR model into the Greenwood and Williamson framework (1966) that will be discussed later. Their results on a Perspex-rubber interface are used here to set an arbitrarily large reference value of μ , i.e., $\mu = 100$, from which that of other material interfaces can be derived under the additional assumption that the maximum adhesive stress, σ_o , remains constant. In particular, a value as small as $\mu = 0.079$ is obtained for contacts between Perspex and steel with relevant parameter values shown in Table 2. This approach is motivated by the lack of sufficient information on the physical parameters characterizing the micromechanics of contacts considered in this work, that is to say, contacts with $\mu < 1$. Figure 7 illustrates the dependence of the normalized force, $F^*(\delta^* | \mu) = F(\delta^* | \mu) / F_c$, on the normalized relative approach, $\delta^* = \delta / \delta_c$, where $F_c = (2\pi R \Delta\gamma)$, $\delta_c = (\beta^2 / R)$, and $\beta = (R^2 \Delta\gamma / E')^{1/3}$, for $\mu = 0.079$. With this normalization, the maximum normalized tensile force, \bar{F} , varies from 1 for $\mu = 0$ to $\bar{F} = 0.75$ for $\mu \rightarrow \infty$. In particular, for $\mu = 0.079$, $\bar{F} \cong 0.981$, that is to say, it differs from the value typical of a rigid contact by about 2 percent.

According to the GJ model, there is no long-range interaction. Thus, during approach, the first contact between the spheres is established when $\delta^* = 0$. At that point, an attractive force draws the two bodies together, and a new equilibrium configuration characterized by a finite contact area, and, thus, a finite approach, is established by the balance between the attractive adhesive force and the elastic reaction to it. The application of an additional external compressive force increases the relative approach as in the Hertzian case. Upon unloading, the force-approach relationship retraces the

μ	R (μm)	$\Delta\gamma$ (mJ m^{-2})	δ_c (nm)	F_c (10^{-6} N)
0.079	1	40.	0.37	0.25

Table 2. Physical and geometrical parameters defining the contact.

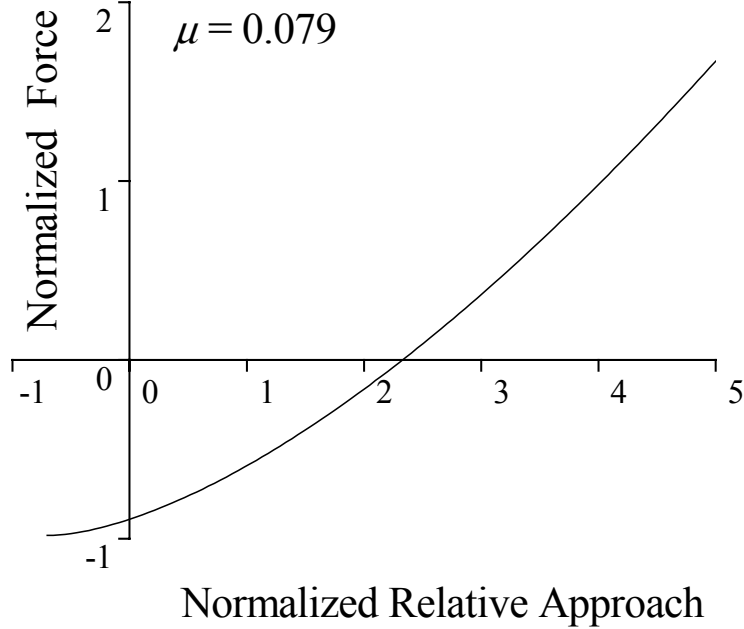


Figure 7. Plot of the force-displacement relationship for a contact between Perspex and steel spheres characterized by the parameters of Table I according to the Greenwood and Johnson model.

loading curve in the opposite direction. Upon unloading, the force-approach relationship retraces the loading curve in the opposite direction. At $\delta^* = 0$, however, the area of the contact as well as its stiffness are still finite. Therefore, in order for a complete detachment to occur, the applied tensile force must be further increased and the contact must be stretched beyond the point at which it was established. If the load on the contact is transmitted by a device having infinite compliance, then the contact breaks when its stiffness becomes null, that is to say, when the tangent to the curve in Fig. 7, is parallel to the δ^* axis. At this point, $\delta^* = \bar{\delta}$ and $F^*(\bar{\delta} | \mu) = \bar{F}$. This situation closely resembles that occurring during a wave scattering event in which an interface is partially closed by an instrument controlling the load, and the contacts are formed and broken by the stress carried by the wave field.

2.3.2 Rough surfaces in contact

The Greenwood and Williamson's (1966) model is reviewed here to be adapted to the case of present interest. Following Brown and Scholz (1985), the original problem is transformed into that of an auxiliary surface (the composite surface) pressed against an infinitely rigid flat (see Fig. 1). The relationship between the applied pressure, P , and the relative approach, Δ , between the mean planes of the rough surfaces in contact can be written as follows

$$P(\Delta) = n \int_{Z_o - \Delta, \alpha_0, \beta_0}^{Z_o, \alpha_1, \beta_1} F(z - Z_o + \Delta | \lambda_1, \lambda_2, \dots) \phi(Z_o - z) \phi(\lambda_1) \eta(\lambda_2) \dots dz d\lambda_1 d\lambda_2 \dots \quad (26)$$

In Eq. (26), $\phi(\cdot)$ is the probability density function of the peaks of the auxiliary, composite surface. The latter is defined by an appropriate algebraic combination of the profiles of the two rough surfaces of interest, which maps the individual contacts between the asperities of the two surfaces into the peaks of the composite one. Thus, $\phi(Z_o - z) dz$, which gives the number of peaks with height between z and $z + dz$ above the mean plane of the composite surface, represents also the number of contacts formed in this interval. Z_o is the maximum height of the asperities of the composite surface, and, thus, $\phi(Z_o - z) = 0$ for $z > Z_o$. In equation (1), n is the number of contacts per unit area, and $F(\cdot)$ is the force law between asperities, which depends on their relative approach, $\delta = z - Z_o + \Delta$, as well as on additional contact parameters, $\lambda_i, i = 1, 2, \dots$. The values of the latter for each contact are generally unknown, and, thus, are to be considered stochastic variables with probability density functions $\phi(\cdot), \eta(\cdot), \dots$, respectively. The integration over z is carried out between the actual position of the flat surface with respect to the mean plane of the composite surface, $Z_o - \Delta$, and the initial position of the same surface for $P = 0, Z_o$. The integrals over the other stochastic variables are also evaluated over appropriate ranges of values.

Introducing the force law of the GJ model in Eq. (26), the latter becomes

$$P(\Delta^*) = 2\pi n \int_{0, R_0, \Delta\gamma_0}^{\Delta^*, R_1, \Delta\gamma_1} R \Delta\gamma F^*(\Delta^* - t^* | \mu) \phi(t^*) \phi(R) \eta(\Delta\gamma) dt^* dR d(\Delta\gamma) \quad (27)$$

In Eq. (27), the new non-dimensional variable $t^* = (Z_o - z) / \delta_c$ has been introduced, and $\lambda_i, i = 1, 2$, have been identified with R and $\Delta\gamma$, respectively. Consistently, $\Delta^* = \Delta / \delta_c$. For the sake of conciseness, the Tabor parameter has replaced R and $\Delta\gamma$ in the expression of the force law. The distribution of the values of R has been assumed to be independent of the asperity height z , and the surface energy $\Delta\gamma$ which depends only on the nature of the materials, has been taken to be the same for all the contacts. Thus, $\eta(\cdot) = \delta(\cdot)$, where $\delta(\cdot)$ is the delta of Dirac, and Eq. (27) becomes

$$P(\Delta^*) = 2\pi n \Delta\gamma \int_{0, R_0}^{\Delta^*, R_1} R F^*(\Delta^* - t^* | \mu) \phi(t^*) \phi(R) dt^* dR \quad (28)$$

Fuller and Tabor (1975) developed a similar model in which the force law of the JKR model was used. In their work, they implicitly assumed that all the contacts have the same composite radius of curvature, R . Although this is a rather drastic approximation, the effects of which will be discussed later, it will be adopted even in this work for the sake of simplicity. Therefore, setting $\phi(\cdot) = \delta(\cdot)$ in Eq. (28) yields

$$P(\Delta^*) = 2\pi n R \Delta\gamma \int_0^{\Delta^*} F^*(\Delta^* - t^* | \mu) \phi(t^*) dt^* \quad (29)$$

Following Baltazar *et al.* (2002), the probability density $\phi(t^*)$ is chosen to be a chi-squared probability density function as given by Eq. (3) in Section 2.2.1.

Having brought the two surfaces to a maximum normalized approach Δ_{\max}^* at the end of loading phase of the first cycle, the relationship between the applied pressure, P , and the normalized relative approach, Δ^* , during unloading is given by

$$P(\Delta^*) = 2\pi n R \Delta \gamma \int_0^{\Delta^*+D} F^*(\Delta^* - t^* | \mu) \varphi(t^*) dt^*, \quad (30)$$

where $D = \Delta_{\max}^* - \Delta^*$, if $0 < \Delta_{\max}^* - \Delta^* < \bar{\delta}$, and $D = 0$, if $\Delta_{\max}^* - \Delta^* > \bar{\delta}$. The inclusion of D in the upper limit of integration is to account for the stretching of the peaks that had been formed last during the preceding loading phase of the cycle.

The main interest of this investigation is in the dynamic behavior of the interface when it is subjected to a cyclic loading. Thus, if Δ_{\min}^* is the relative approach at the end of the unloading phase of the cycle, the pressure-approach relationship during all the following loading phases is given by

$$P(\Delta^*) = 2\pi n R \Delta \gamma \int_0^{\Delta^*+D} F^*(\Delta^* - t^* | \mu) \varphi(t^*) dt^*, \quad (31)$$

where $D = \bar{\delta} - \Delta^* + \Delta_{\min}^*$, if $0 < \Delta^* - \Delta_{\min}^* < \bar{\delta}$, and $D = 0$, if $\Delta^* - \Delta_{\min}^* > \bar{\delta}$. The lower limit of integration accounts for the effect of contacts that are under tension at the end of the unloading cycle, and are now progressively set under increasing compression again during the current compressive phase of the cycle.

Let the interface be subjected to a static load P_o upon which an oscillating component, ΔP , is superimposed. Figure 8 illustrates an example of such a pressure-approach relationship for an interface between Perspex and steel. The Young modulus of the Perspex is $E_1 = 2.85$ GPa, and that of steel is $E_2 = 192$ GPa, while the values of the Poisson modulus are $\nu_1 = 0.4$ and $\nu_2 = 0.28$, respectively. The value of $\Delta \gamma = 40$ mJ/m² for the surface energy change is used (Fuller and Tabor, 1975), while that of the peak density, n , of the composite surface is obtained by employing the approximation $n = 0.1/R\sigma$, which was found experimentally by Fuller and Tabor (1975). In addition, the rms roughness of the composite surface is $\sigma = \sqrt{\sigma_1^2 + \sigma_2^2} = 30$ nm, where σ_1 and σ_2 are the rms roughness of the two surfaces. A number of degrees of freedom, n , equal to 10 completes the characterization of the probability distribution density of the composite asperities. The parameter values characterizing the individual contacts are those reported in Table 2. In Fig. 8, the pressure, P , is normalized by $P_c = 2\pi n R \Delta \gamma$: $P^* = P/P_c$.

For the purpose of the present investigation, the most important feature displayed by Fig. 8 is the hysteresis with end-point memory displayed by the plot of the normalized pressure, P^* , versus the normalized relative approach, Δ^* . Such hysteretic behavior is caused by the forces of adhesion. This fact can be better understood by the analysis of the interfacial stiffness, K_N , as a function of the relative approach (Fig. 9). The stiffness, K_N , which in Figure 4 is normalized with respect to $K' = F_c / \delta_c$, is defined mathematically by the first derivative of the pressure with respect to the relative

approach, $K_{N,o} = (\partial P / \partial \Delta)_{\Delta_o}$ at $\Delta = \Delta_o$, where Δ_o is the value of the approach at equilibrium. In Fig. 8, the behavior of K_N as the interface reaches its equilibrium during

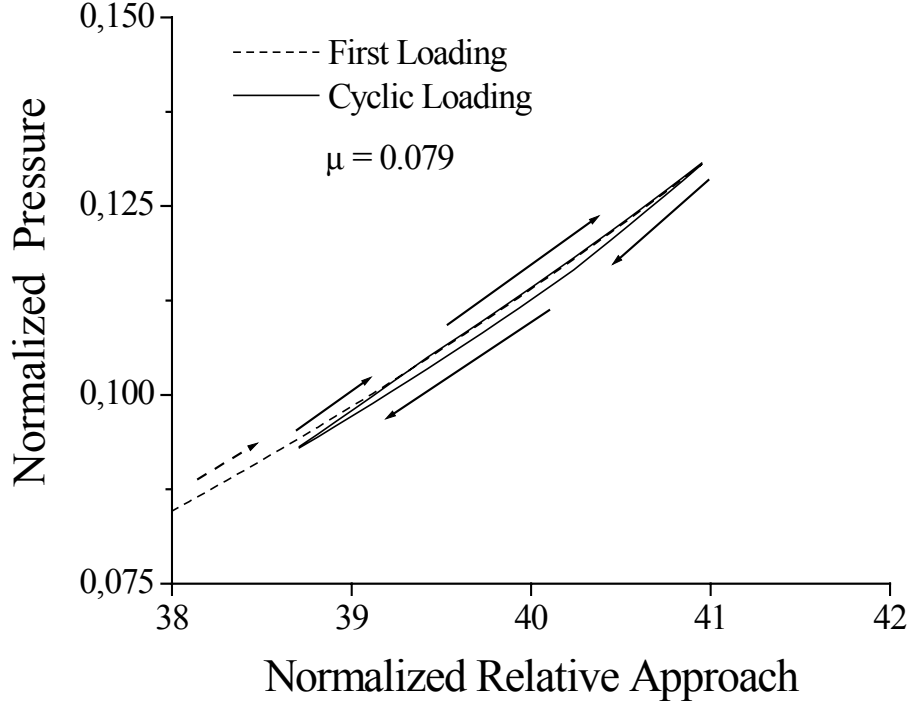


Figure 8. An example of the hysteresis loop displayed by the pressure-relative approach relationship of an interface between two rough surfaces in contact when subjected to a cyclic load. The interface separates two halfspaces of Perspex and steel, and the parameters characterizing the contacts are given in Table 2.

the first loading is illustrated by the dotted line. When probed dynamically by a periodic perturbation producing a variation of the normalized approach at equilibrium not exceeding the normalized distance $\bar{\Delta}/2 = \delta_c \bar{\delta}/2$, the stiffness of the interface undergoes a discontinuous positive variation after reaching its maximum value at the end of the first compressive phase. After such an event, it varies continuously along the upper side of the unloading cycle (path between the points A and B in Fig. 9). Thus, for small variations of the instantaneous relative approach from its value at equilibrium, the stiffness displayed by the interface during the following cycles is larger than that at equilibrium, $K_{N,o}$, and can be approximated by a linear expansion in $\delta\Delta$: $K_N \cong K_o + K_1 \delta\Delta$. The constant term K_o can still be evaluated as the first derivative of the pressure with respect to the relative approach, as in the case of $K_{N,o}$, $K_o = (\partial P / \partial \Delta)_{\Delta_o}$. However, care must be taken to perform this derivative after the first compressive cycle has terminated. Similarly, $K_1 = (\partial^2 P / \partial \Delta^2)_{\Delta_o}$.

For variations of the instantaneous relative approach having amplitude $\delta\Delta$ such that $\delta\Delta = \bar{\Delta}/2$, at each turning point in a cycle and at a distance equal to $\bar{\Delta}$ from them, the stiffness undergoes sudden discontinuous variations during all cycles following the first one. The positive jump at the beginning of the unloading phase is due to the stiffening reaction accompanying the stretching of the contacts last formed during the

previous loading phase; that at the opposite end of the cycle is determined by the onset of the removal of the contacts under tension. The negative jump during unloading

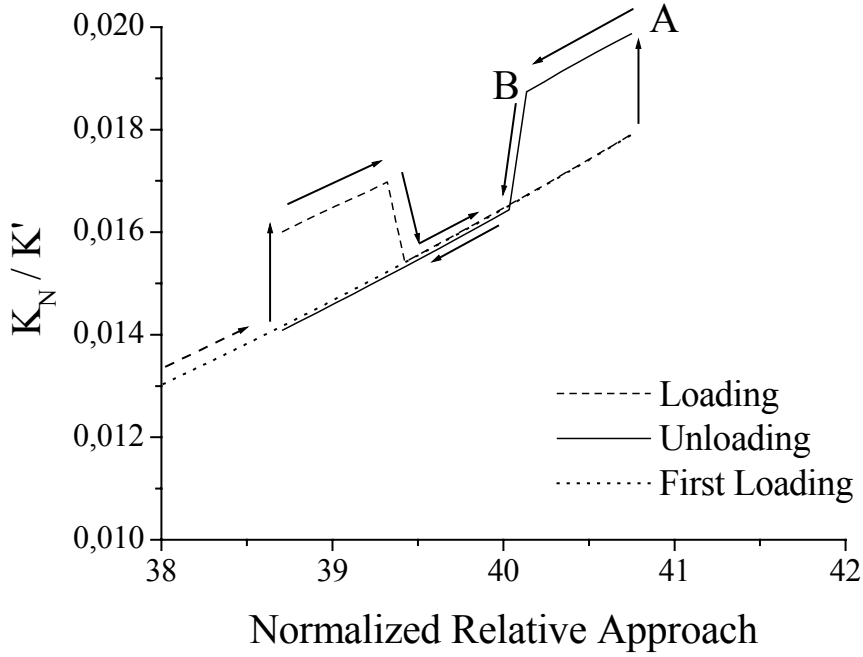


Figure 9. Dependence of the normal interfacial stiffness on the interface relative approach. The normalization constant is $K' = N p_c / \delta_c$, where N is the number of contacts per unit area. The points A and B indicate the path along which the system evolves when the maximum variation of the interface opening displacement is smaller than $\bar{\Delta}/2$. The interface is that of the previous figure.

occurs when the first rupture of contacts takes place, while that during the loading cycle is determined by the completion of the removal of all the contacts under tension. In conclusion, during dynamic loading, the interface stiffness can be approximated by the following expression

$$K_N(\Delta = \Delta_o + \delta\Delta) = K_0 + K_1 \delta\Delta - K_2' H\left(\text{sgn}\left(-\frac{\partial\Delta}{\partial t}\right)\right) H(\Delta_{\max} - \bar{\Delta} - \Delta) - K_2'' H\left(\text{sgn}\left(\frac{\partial\Delta}{\partial t}\right)\right) H(\Delta - \Delta_{\min} - \bar{\Delta}), \quad (32)$$

in which, in addition to the linear expansion already considered, two products of step functions have been introduced. In the first product, the first step function is non-zero only during the unloading phase of a cycle, while in the second one, the first step function is non-zero during the loading phase. The second step functions in each product describe the negative jumps of the stiffness occurring during a cycle. The coefficients K_2' and K_2'' measure the stiffness variations taking place during the jumps.

The behavior of the stiffness just discussed is another manifestation of the hysteresis with end-point memory affecting the pressure-approach relationship, and demonstrates the similarity between the dynamics of this type of interface and that of a

fictitious hysteretic elastic unit (HEU) of the Preisach-Mayergoyz space. Both can exist in two dynamic states, and the transitions between the latter are determined by threshold values of the independent variable, as well as by the history of the state. In addition, contacts between asperities are material features with typical mesoscopic dimensions. To the best of this author's knowledge, this is the first example of a real mechanical interface or bond between solid bodies which can be shown to behave like a hysteretic elastic unit of the Preisach-Mayergoyz (P-M) model used to simulate the propagation of acoustic waves in materials with hysteretic properties (Guyer and Johnson, 1999).

2.3.3 Wave reflection and transmission

In this section, the effective boundary conditions needed to describe the scattering of a longitudinal wave by an interface such as those described above are formulated. The propagation direction of the incident wave is assumed to be normal to the interface, and the boundary value problem is solved by means of a standard perturbation approach.

From Eq. (32), the behavior of the normal stiffness of the interface as a function of the interface opening displacement (IOD) oscillation, Δu is approximated by the following function

$$K_N(\Delta u) = K_0 - K_1 \Delta u - K_2' H\left(\text{sgn}\left(\frac{\partial \Delta u}{\partial t}\right)\right) H(\Delta u + \Delta u_{\max} - \bar{\Delta}) - K_2'' H\left(\text{sgn}\left(-\frac{\partial \Delta u}{\partial t}\right)\right) H(\Delta u_{\max} - \bar{\Delta} - \Delta u), \quad (33)$$

where $\delta \Delta = -\Delta u$, $\Delta u_{\min} = \Delta_o - \Delta u_{\max}$, and the symbol Δu_{\max} denotes the amplitude of the interface opening displacement's oscillation, Δu . Therefore, the first boundary condition to be enforced at the interface is

$$\sigma_{33}(0^+, t) = K_N(\Delta u) \Delta u, \quad (34)$$

where $K_N = K_N(\Delta u)$ is given by Eq. (33), $\Delta u(t) = u(0^+, t) - u(0^-, t)$, and $u(0^+, t)$ and $u(0^-, t)$ are the total displacement fields on the positive and negative side of the interface, respectively. The second boundary condition requires the normal stress to be continuous across the interface,

$$\sigma_{33}(0^+, t) = \sigma_{33}(0^-, t). \quad (35)$$

The incident wave is assumed to propagate in the half-space $z < 0$. The Lamé constants of the negative half-space are λ^- and μ^- , while λ^+ and μ^+ are those of the positive half-space. If A_{in} is the amplitude of the incident wave, the total fields in the negative and positive half-spaces can be written in terms of two new non-dimensional functions $u^-(z, t) = A_{in} \xi^-(z, t)$, and $u^+(z, t) = A_{in} \xi^+(z, t)$, respectively. Introducing the following

non-dimensional variables, $\eta = k^- z$, where k^- is the longitudinal wave number in the negative half-space, and $\tau = \omega t$, where ω is the angular frequency of the incident wave, the boundary conditions for this problem can be cast in the following form

$$k^- (\lambda^+ + 2\mu^+) \frac{\partial \xi^+}{\partial \eta} = K_0 \Delta \xi - K_1 A_{in} \Delta \xi^2 - K_2' \left[H \left(\text{sgn} \left(\frac{\partial \Delta \xi}{\partial \tau} \right) \right) H(\Delta \xi + \Delta \xi_{\max} - \bar{\Delta}) + \theta H \left(\text{sgn} \left(-\frac{\partial \Delta \xi}{\partial \tau} \right) \right) H(\Delta \xi_{\max} - \bar{\Delta} - \Delta \xi) \right] \Delta \xi, \quad (36)$$

$$(\lambda^+ + 2\mu^+) \frac{\partial \xi^+}{\partial \eta} = (\lambda^- + 2\mu^-) \frac{\partial \xi^-}{\partial \eta}. \quad (37)$$

In Eq. (36), $\bar{\Delta}$ has been redefined as $\bar{\Delta} = \bar{\Delta}/A_{in}$, and $\theta = K_2''/K_2'$. The solutions are sought in the form of a perturbation series in two small parameters, ε_1 and ε_2

$$\xi^-(\eta, \tau) = \frac{1}{2} \{ \exp[i(\tau - \eta)] - R \exp[i(\tau + \eta)] - \varepsilon_1 U_1(\eta, \tau) - \varepsilon_2 U_2(\eta, \tau) + \dots C.C. \}, \quad (38)$$

$$\xi^+(\eta, \tau) = \frac{1}{2} \{ T \exp[i(\tau - \kappa \eta)] + \varepsilon_1 V_1(\eta, \tau) + \varepsilon_2 V_2(\eta, \tau) + \dots C.C. \}, \quad (39)$$

in which R and T are the linear reflection and transmission coefficients of the incident wave, $\varepsilon_1 = K_1 A_{in}/K_0$, $\varepsilon_2 = K_2'/K_0$, $\kappa = (C_L^-/C_L^+)^2$, where the C_L s are the longitudinal phase velocities in the two half-spaces, and C.C. represents the complex conjugate.

In the series expansions of Eq. (38) and (39), the two perturbation parameters ε_1 and ε_2 are treated as independent of each other regardless of the fact that the physics of the interface is unique. Regardless of the nature of the connection between the two parameters, such an approach is justified in view of the additivity of the nonlinear corrections to the interfacial stiffness determined by them. In fact, accounting for the relationship between ε_1 and ε_2 leads to a system of boundary conditions for the first order displacement fields in which the ‘driving force’ is the linear superposition of the contributions due to hysteresis and to the term which is quadratic in the IOD. Therefore, the first-order correction of the displacement fields can be decomposed into two components each of which is separately determined by the corresponding nonlinear term of the interfacial stiffness. In conclusion, for the purpose of finding the first order correction to the displacement fields, ε_1 and ε_2 can be regarded as independent of each other.

Figure 10 illustrates an example of the dependence of the two nonlinear parameters ε_1 and ε_2 and of $\varepsilon_2' = \theta \varepsilon_2$ on the normalized stiffness $K_0/(Z^- \omega)$, where $Z^- = \rho^- C_L^-$, the product of the mass density of the medium and the phase velocity of the propagating wave, is the acoustic impedance of Perspex, and ω is the angular frequency of the incident wave. The amplitude of the latter is assumed to be $A_{in} = 2$ nm. These data are evaluated for an interface between Perspex and steel with composite roughness $\sigma = \sqrt{\sigma_1^2 + \sigma_2^2} = 30$ nm, where σ_1 and σ_2 are the rms roughness of the two

surfaces, and by a probability distribution density with a number of degrees of freedom $N = 10$. All three parameters are shown to diverge as the interface opens. In addition, ε_2 and $\varepsilon'_2 = \theta\varepsilon_2$ go suddenly to zero in the neighborhood of $K_0/Z^-\omega = 8$, where, in this particular case, the amplitude of the IOD variation becomes smaller than $\bar{\Delta}$.

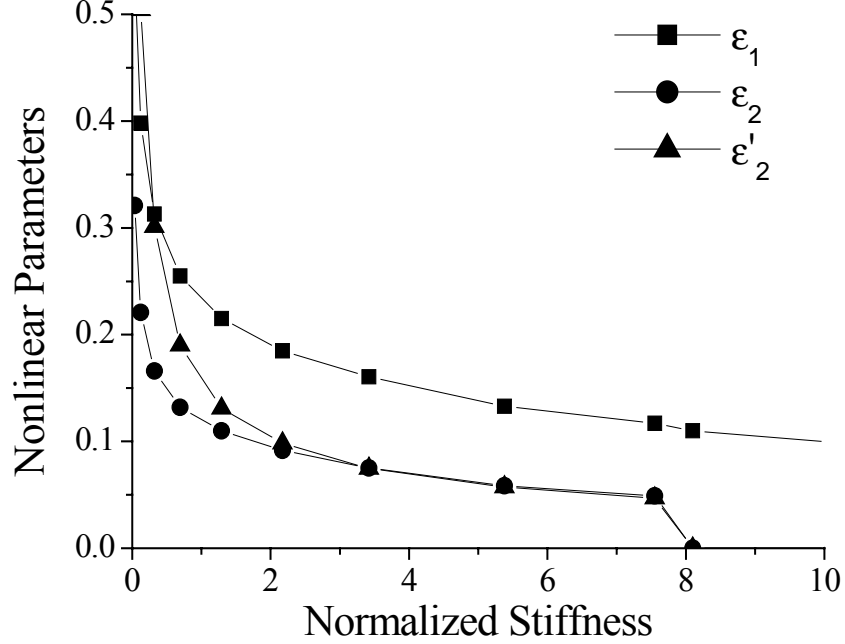


Figure 10. Nonlinear perturbation parameters versus normalized stiffness. All three parameters diverge as the interface opens. Those controlling the nonlinearity due to adhesion suddenly go to zero around $K_0/Z^-\omega = 8$, when the maximum variation of the interface opening displacement becomes smaller than $\bar{\Delta}/2$. The amplitude of the incident wave is $A_{in} = 2$ nm.

Introducing Eq. (38) and (139) in the boundary conditions, and separating the terms according to their dependence on the perturbation parameters ε_l and ε_2 , the following boundary conditions for the zero-th and first order solutions are obtained

0th order system:

$$k^-(\lambda^+ + 2\mu^+)(-i\kappa T) = K_0(T - 1 + R), \quad (40)$$

$$(\lambda^+ + 2\mu^+)\kappa T = (\lambda^- + 2\mu^-)(1 + R), \quad (41)$$

First order system in ε_l :

$$k^-(\lambda^+ + 2\mu^+) \frac{\partial V_1}{\partial \eta} + C.C. = K_0 \{V_1 + U_2 + C.C. - \frac{1}{2}(T-1+R)^2 \exp[i2\tau] - |T-1+R|^2 + C.C.\}, \quad (42)$$

$$(\lambda^+ + 2\mu^+) \frac{\partial V_1}{\partial \eta} + C.C. = -(\lambda^- + 2\mu^-) \frac{\partial U_1}{\partial \eta} - C.C. \quad (43)$$

First order system in ε_2 :

$$k^-(\lambda^+ + 2\mu^+) \frac{\partial V_2}{\partial \eta} + C.C. = K_0 \{V_2 + U_2 + C.C. + \left[H\left(\text{sgn}\left(\frac{\partial \Delta \xi_0}{\partial \tau}\right)\right) H(\Delta \xi_0 + \bar{\Delta}_{\max} - \bar{\Delta}) + \theta H\left(\text{sgn}\left(-\frac{\partial \Delta \xi_0}{\partial \tau}\right)\right) H(\bar{\Delta}_{\max} - \bar{\Delta} - \Delta \xi_0) \right] \times (\Delta \xi_0 + C.C.)\}, \quad (44)$$

$$(\lambda^+ + 2\mu^+) \frac{\partial V_2}{\partial \eta} + C.C. = -(\lambda^- + 2\mu^-) \frac{\partial U_2}{\partial \eta} - C.C. \quad (45)$$

In Eq. (44), the arguments of the step functions have been approximated by using the solutions of the zero-th order system, which is a reasonable approximation as long as the nonlinearity of the interface is small. The solutions of the zero-th order system are

$$R = -\frac{i\omega Z^- - K_0 \left(1 - \frac{Z^-}{Z^+}\right)}{i\omega Z^- + K_0 \left(1 + \frac{Z^-}{Z^+}\right)}, \text{ and } T = \frac{Z^-}{Z^+} R, \quad (46)$$

where $Z^\pm = (\rho C_L)^\pm$ are the longitudinal acoustic impedances of the positive and negative half-spaces, respectively. The symbol ρ represent the mass density of the medium. The solutions V_2 and U_2 of the first first-order system are found by employing R and T to evaluate the terms on the right-hand side of Eq. (44) which contain them. Such terms are further expanded in a Fourier series, so that Eq. (44) can be recast as follows

$$k^-(\lambda^+ + 2\mu^+) \frac{\partial V_2}{\partial \eta} + C.C. = K_0 \left\{ V_2 + U_2 + C.C. + c_0 + \sum_n c_n e^{in\tau} + C.C. \right\}. \quad (47)$$

This equation, together with Eq. (45) is solved by expanding V_2 and U_2 in Fourier series,

$$U_2(\eta, \tau) = \sum_n A_n e^{in(\tau+\eta)}, \text{ and } V_2(\eta, \tau) = \sum_n B_n e^{in(\tau-\kappa\eta)},$$

and by introducing such representations of the unknown solutions in the boundary conditions. Simple algebra leads to the following expressions for the coefficients of the series

$$A_n = -\frac{K_0 c_n}{in\omega Z^- + K_0 \left(1 + \frac{Z^-}{Z^+}\right)}, \text{ and } B_n = \frac{Z^-}{Z^+} A_n . \quad (48)$$

By using the harmonic balance methods, the solutions of the boundary value problem of Eq. (42) and (43) are found to comprise terms that are constants and others that contain the second harmonic component. The amplitudes of the first ones are

$$U_{1,0} = \frac{|T-1+R|^2}{1 + \frac{Z^-}{Z^+}}, \text{ and } V_{1,0} = \frac{Z^-}{Z^+} U_{1,0} \quad (49)$$

while those of the second harmonic components are

$$U_{1,2} = \frac{K_0}{2} \frac{(T-1+R)^2}{i2\omega Z^- + K_0 \left(1 + \frac{Z^-}{Z^+}\right)}, \text{ and } V_{1,2} = \frac{Z^-}{Z^+} U_{1,2} . \quad (50)$$

Note the positive value of both $U_{1,0}$ and $V_{1,0}$. This result is consistent with the fact that the quadratic nonlinearity describes a spring that becomes stiffer under compression.

Figure 11 illustrates an example of normalized spectrum of the higher harmonics generated upon scattering of an incident wave with amplitude $A_{in} = 2$ nm, frequency $f = 1$ MHz, and propagating in the Perspex halfspace. The amplitude of the incident wave is used as normalization constant. The interface is that of Figure 5 with a value of the normalized stiffness equal to 1.29. To the first-order approximation, and when hysteresis is activated – indeed, for values of $\Delta\xi_{\max} < \bar{\Delta}/2$ only the classical nonlinear corrections are present – the amplitude of all the higher harmonics is a function of A_{in}^2 , as experimentally verified in damaged materials, at least for the third harmonic component. In the same approximation, the amplitude of the even harmonics of an order higher than the second depends also on the departure of θ from unity, that is to say, on the loss of symmetry between the compressive and the tensile parts of each cycle.

It is important to point out the remarkable resemblance between the spectra in Fig. 11 and those predicted by Van den Abeele *et al.* (1997) in their theoretical investigation on nonlinear propagation of acoustic waves in nonlinear media, in which the P-M model was used to characterize the type and degree of nonlinearity. Meegan *et al.* (1992) and TenCate *et al.* (1996) also reported measured spectra of a waves propagating in sandstone and other geomaterials, which bear a strong resemblance to those of Fig. 6. In particular, the slow decay of the amplitude of the higher harmonics

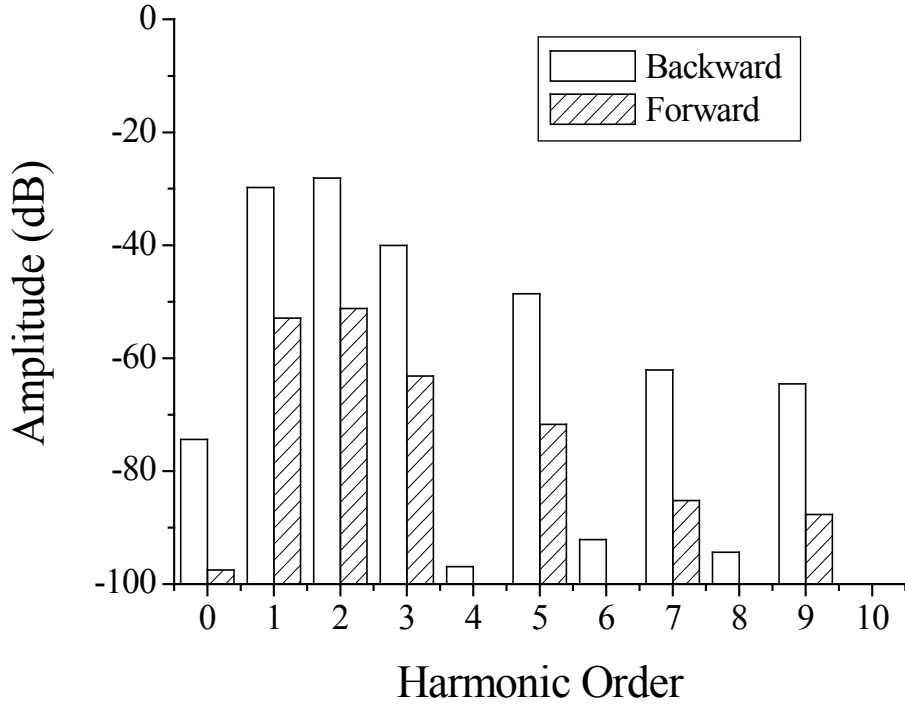


Figure 11. Normalized spectrum of nonlinear waves that are scattered forward and backward by the interface considered in Figures 3 and 4, and which is characterized by a normalized linear component of the interface stiffness $K_0/Z^-\omega = 1.29$.

together with the dominant presence of the odd components seem constitute the acoustic signature of an hysteretic interface with end-point memory.

Finally, Fig. 12 illustrates the dependence of the second and third harmonics on the normalized interface stiffness, or, in other terms, on the interface opening. As the contacts begin to form, both components increase until they reach a maximum value near $K_0/Z^-\omega = 1$. However, for very small values of K_0 , the parameters ε_1 and ε_2 exceed the value of 0.3 rendering the approximation no longer accurate. The numerical estimates of the second and third harmonic amplitudes beyond the range of validity of the approximation are reported nonetheless to illustrate the trend the actual solutions are expected to follow. Note that the dependence of the amplitude of the third harmonic on the normalized stiffness is considerably weaker than that displayed in the case of surfaces in contact and subjected to an oscillating tangential load. However, as already remarked in the discussion of Fig. 10, the amplitude of the third harmonic goes to zero when the amplitude of the IOD variation becomes smaller than $\bar{\Delta}$.

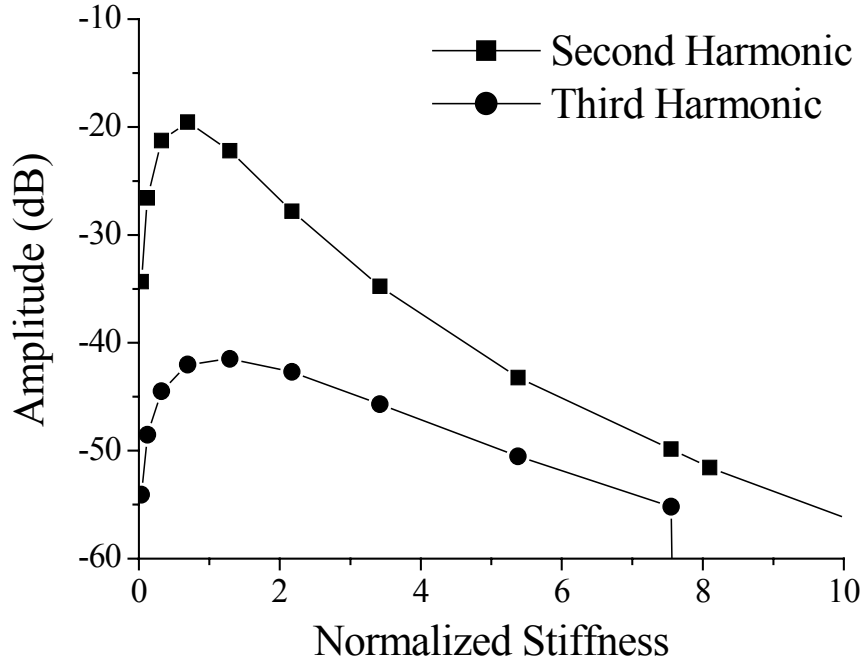


Figure 12. Normalized amplitude of the second and third harmonic waves versus the normalized interfacial stiffness for the interface considered in the previous two figures.

2.3.4 Concluding remarks

A few comments are still in order to complete the description of the present model. First of all, the mechanics of the contacts considered in this work does not account for any long-range interaction which may exist in real contacts, leading two asperities to form a contact when δ is still negative (the 'jump-on' phenomenon (Greenwood (1998), Inagaki *et al.* (2002))). Such an event is accompanied by some energy loss following the impact, which a rigorous theoretical treatment should account for. However, as long as only a small percentage of the asperities is involved, as required by the Greenwood and Williamson approximation, such a mechanism is expected not to alter significantly the conclusions presented here since it involves a small fraction of the energy carried by the acoustic wave.

Equations (29, 30, and 31) relating the pressure, P , to the relative approach, Δ , have been obtained under the assumption that all the asperities have the same radius of curvature. This assumption is unlikely to be satisfied by normal, rough surfaces, and, therefore, the radius of curvature in the equations just cited has to be weighted by its own probability density function. Note also that contacts with different radii of curvature are characterized by different values of the Tabor parameter, μ . Consequently, the stiffness of the interface is expected to undergo sudden transitions only at the end-points of each cycle (see Fig. 9), the remaining two transitions becoming continuous, in view of the fact that contacts having different radii of curvature come apart at different values of the distance $\bar{\delta}$. The width of the regions where such continuous transitions occur closely follows that of the probability density function of the radius of curvature. Finally, under these conditions, the spectrum of a wave

scattered by such an interface is expected to be characterized by a content of higher harmonics that is less pronounced than that shown in Fig. 11.

As the Tabor parameter, μ , goes to zero by maintaining a constant values of the surface energy, $\Delta\gamma$, the present model of the mechanics of two rough surfaces in contact is expected to approach that by Maugin (1991), which was developed by using the Derjaguin, Muller, Toporov force law of individual contacts. According to the latter model, the bodies in contact do not deform in the annular area, which surrounds the contact and where the force of adhesion acts. Furthermore, the maximum adhesive force is that predicted by Bradley. If the limit $\mu \rightarrow 0$ is achieved by letting the maximum adhesive stress, σ_o , become progressively smaller, the case described by Pecorari (2003) of a nonlinear purely elastic interface is recovered.

The limitation of the present work notwithstanding, the similarity of the spectra of Fig. 11 and those experimentally observed in geomaterials, or predicted by phenomenological theories based on the P-M model can hardly be considered coincidental. In fact, although it is reasonable to assume that more than one mechanism concurs to determine the nonlinear behavior of a complex medium with microstructure and/or damage, the presence of soft bonds and microcracks in rocks or other composite materials provides ample opportunity for contact nonlinearity to play a significant role. Furthermore, since elastic nonlinearity cannot explain the magnitude of the amplitude of the higher amplitude (Pecorari, 2003), adhesion becomes a serious candidate to be considered as a fundamental mechanism behind the nonclassical nonlinear physical behavior of hysteretic materials with end-point memory.

Finally, the micromechanics model presented in this work may also provide the key to interpreting the excess linearity observed in partially saturated rocks (Van den Abeele *et al.* (2002)). In fact, the mechanics of adhesion between soft bodies can be used to reasonably describe the interaction between asperities covered by very thin layers of water or other liquids. This conjecture seems to be supported also by a theoretical investigation by Goryacheva and Makhovskaya (2002). Should this be the case, then stress-corrosion cracks formed in pipes containing corrosive liquids at high pressure may also be expected to display nonlinear acoustic properties which resemble those described in this work.

2.4 Scattering by a surface-breaking crack

2.4.1 Introduction

Material components containing cracks respond to an external dynamic perturbation in a nonlinear manner (Solodov, 1998, Solodov, Krohn, Busse, 2002). For instance, when insonified by a harmonic wave, the spectrum of the acoustic response of a cracked sample has been shown to displays higher-order harmonic components, which are not found in samples without cracks. Similarly, if a component containing a partially closed crack is tested simultaneously by two harmonic waves of frequencies f_1 and f_2 , with $f_1 \gg f_2$, signals are generated within the sample, which contain side-band

components at frequencies $f_1 \pm f_2$. These, again, are not found in the acoustic fields generated by scattering events in material components without cracks.

An even richer phenomenology (Solodov and Korshak, 2002) can be observed when the amplitude of the excitation is increased beyond the threshold value at which clapping between the crack's faces is activated. For example, the generation of subharmonic components, which is the first step towards a chaotic regime of vibration, can be observed by progressively increasing the excitation amplitude. Nonlinear effects caused by the dissipation of the acoustic energy have also been reported in experiments conducted on cracked glass samples (Zaistev, Gusev, and Castagnede, 2002, Zaistev, Gusev, and Castagnede, 2003)

Such experiments are often performed with continuous waves at frequencies that are well below the MHz range, so that the wavelength of the waves propagating within the inspected component is of the order of several centimeters. As the whole volume of the material is insonified, and the acoustic response is commonly detected by using a stationary sensor, defect's localization under such experimental conditions is a very difficult task.

An important variation of this approach is that developed by Krohn *et al.* (Krohn, Stoessel, Busse, 2002) in which the local response of a composite plate to a low-frequency, large-amplitude acoustic wave source is detected by a scanning laser interferometer. In these experiments, the plate's thickness is much smaller than the wavelength of the probing acoustic wave. The large values of the wave amplitude utilized in these experiments suggest that the mechanism responsible for the nonlinear response of the plate is clapping between the faces of the delamination. This hypothesis is further supported by the presence of harmonics of very high order in the scattered acoustic field. Images of the plate formed by displaying the amplitude variation of higher order harmonics show a feature of great importance for practical applications: the highly localized nonlinear response of the defect, which decays by as many as 20 dB as the observation point moves away from the defect. A convincing explanation of such an interesting phenomenon has yet to be provided.

A few authors have developed models, which predict the nonlinear response of cracks with faces interacting with each other. Achenbach and Norris (1982) have analyzed the effect of clapping on the linear response of a crack insonified by an incident wave. Boundary conditions along the crack's faces, which require the continuity of the total displacement when the crack is closed, and set the total applied stress to zero when the crack is open, have been used. Hirose and Achenbach (1992) have developed a sophisticated mathematical approach to modeling nonlinear scattering by a circular crack with clapping faces. The time evolution of the clapping faces is followed by numerically solving an appropriate integral equation, the solution of which is used to evaluate the scattered field in the space-time domain. The harmonic content of the scattered field is recovered via Fourier analysis of the latter. A similar approach has also been adopted by Hirose (1994) who employs more realistic boundary conditions at the crack's face. In fact, Hirose considers the interaction between the crack's faces to occur only at discrete locations and at instants that are determined by the time evolution of the applied load, by the crack's initial conditions, and by the topography of the two surfaces. Donskoy, Sutin, and Ekimov (2001) have proposed a simplified mathematical scheme to account for the effect of the nonlinearity introduced by Hertzian contacts between the crack surfaces that are assumed to be rough and nonconforming. To this end, they have used the spring model¹¹ for imperfect interfaces

to formulate the nonlinear boundary conditions at the surface of the crack. Thus, the dynamics of a collection of contacts is simulated by that of two distributions of nonlinear springs having normal and tangential stiffness constants, K_N and K_T , respectively. Donskoy *et al.* (2001), however, have considered only the effect of the normal mode of vibration on the nonlinear scattering process.

While, all the theoretical work cited above concerns itself with cracks that are imbedded into the bulk the hosting material component, in this investigation the focus is on the acoustic response of surface-breaking cracks, of which stress-corrosion cracks are typical and extremely important examples. The mathematical description of the problem at hand is provided by an extension of a previous model (Pecorari, 2001) dealing with the linear wave scattering by surface-breaking cracks with faces in partial contact to include the generation of the second harmonic component. As in Donskoy *et al.*'s work, the spring model for imperfect interfaces is employed to incorporate the nonlinear properties of the crack into the boundary conditions enforced on the total scattering field along the crack faces. In this investigation, however, the nonlinear dynamics of rough surfaces in contact is described in terms of a more recent approach (2003). The latter yields the nonlinear dependence of both spring constants, K_N and K_T , on the local relative approach between the crack's faces in terms of both an appropriate force laws for the interaction between asperities in contact and the surface topography. The nonlinear scattering problem is solved by using a standard perturbation technique, the small perturbation parameter naturally arising from the normalization of both the equations of motion and the boundary conditions as a measure of the interface nonlinearity. The dependence of the scattered second harmonic on the type of incident wave, on its frequency, on the interface spring constants, and on the crack depth is investigated. The spatial evolution of the linear and nonlinear components of the scattered field is also evaluated up to distances of the order of ten wavelengths of the incident wave from the crack. A discussion on the relevance of these results on the nondestructive inspection of components containing surface-breaking cracks concludes this work.

2.4.2 Theory

A complete set of boundary conditions to be enforced on the total acoustic field at an interface between two rough surfaces in contact have been derived by Pecorari (2003) under the assumption that the interaction between the asperities is purely elastic. If the interface is assumed to coincide with the plane of equation $x_I = 0$, the boundary conditions are

$$\frac{1}{2}(\sigma_{31}^+ + \sigma_{31}^-) = K_{T,0}\Delta v - K_{T,N}\Delta u\Delta v - \frac{1}{2}K_{T,1}\left[(\Delta v^2 - \Delta v_{\max}^2)\text{sgn}\left(\frac{\partial \Delta v}{\partial t}\right) + \Delta v\Delta v_{\max}\right] \quad (51.a)$$

$$\frac{1}{2}(\sigma_{11}^+ + \sigma_{11}^-) = K_{N,0}\Delta u - K_{N,1}\Delta u^2, \quad (51.b)$$

$$\sigma_{31}^+ = \sigma_{31}^- \quad (51.c)$$

$$\sigma_{11}^+ = \sigma_{11}^-, \quad (51.d)$$

In Eq. (51a-d), u and v are components of the total displacement in the x_1 and x_3 direction, respectively, $\Delta u = (u^+ - u^-)$ and $\Delta v = (v^+ - v^-)$ are the corresponding interface opening displacements, and σ_{ij}^{+-} , with $i, j = 1, 3$, is the ij -th stress component of the stress field acting on the interface. The superscripts + (-) refers to the half-spaces for which x_1 is positive (negative). All the field quantities are to be understood to be functions of time, t . The coefficients K 's, are derived from suitable micromechanics models, which assume the elastic normal and tangential interaction between asperities to be described by Hertz's (Johnson, 1985) and Mindlin and Deresiewicz's models (1953), respectively, of two elastic spheres in contact. Thus, they can be evaluated numerically in terms of the mechanical and topographic properties of the two rough surfaces in contact. The magnitude of K_N and K_T varies with the load applied to the interface, and so does the ratio K_T/K_N , which, however remains of the order of 0.5. The reader who is interested in further details is referred to Baltazar *et al.* (2002), and Pecorari (2003).

To the first order of approximation, the nonlinear effect due to the hysteretic component of the tangential stiffness is shown to be responsible for the generation of higher harmonics of odd order, the magnitude of which is considerably smaller than that of the second harmonic generated by the nonlinearity due to K_N . For this reason, in Eq. (51.a) those terms which are linked to the latter mechanism can be neglected to obtain the following simplified version of nonlinear boundary conditions,

$$\frac{1}{2}(\sigma_{31}^+ + \sigma_{31}^-) = K_{T,0}\Delta v - K_{T,N}\Delta u\Delta v, \quad (52.a)$$

$$\frac{1}{2}(\sigma_{11}^+ + \sigma_{11}^-) = K_{N,0}\Delta u - K_{N,1}\Delta u^2, \quad (52.b)$$

$$\sigma_{31}^+ = \sigma_{31}^-, \quad (52.c)$$

$$\sigma_{11}^+ = \sigma_{11}^-, \quad (52.d)$$

The mathematical formulation of the problem in which an incident wave is scattered by a surface-breaking crack with nonlinear boundary conditions is presented next. The crack is assumed to be positioned on the positive semi-plane of equation $x_1 = 0$, with its mouth placed at the origin of the coordinate system, while its tip reaches a depth d below surface of the medium. The latter occupies the half-space defined by $x_1 \geq 0$.

Following the approach by Achenbach *et al.* (1980) and Mendelsohn *et al.* (1980), the original problem is decomposed into a symmetric and an antisymmetric part, which are solved in the quarter-space $x_1 \geq 0, x_3 \geq 0$. The boundary conditions associated which these problems are,

symmetric problem

$$\sigma_{13}^+ = 0, \quad x_1 = 0, 0 \leq x_3 < \infty, \quad (53.a)$$

$$\sigma_{11}^+ = K_{N,0}\Delta u - K_{N,1}\Delta u^2, \quad 0 \leq x_3 < d, \quad (53.b)$$

$$u = 0, \quad d \leq x_3 < \infty, \quad (53.c)$$

antisymmetric problem

$$\sigma_{11}^+ = 0, \quad x_1 = 0, 0 \leq x_3 < \infty, \quad (54.a)$$

$$\sigma_{13}^+ = K_{T,0} \Delta v - K_{T,N} \Delta u \Delta v, \quad 0 \leq x_3 < d, \quad (54.b)$$

$$v = 0, \quad d \leq x_3 < \infty. \quad (54.c)$$

In Eq. (53.b) and Eq. (54.b), σ_{ij}^+ are the components of the total stress field on the side of the crack facing the quarter-space for which $x_1 > 0$. They include the contribution of the incident wave. In both problems, the components σ_{33} and σ_{31} of the total stress field must be null at the surface $x_3 = 0$. Note that, in view of the continuity of σ_{11} and σ_{31} across the contacting surfaces of the crack as given by Eq. (52.c, d), Eq. (53.b) and Eq. (54.b) can be formulated only in terms of the total stress components on the positive face of the crack.

Since the material half-space supporting the propagation of the acoustic waves is linear, the same equations of motion used by Achenbach *et al.* (1980) and Mendelsohn *et al.* (1980) apply,

$$c_L^2 \frac{\partial^2 u}{\partial x_1^2} + c_T^2 \frac{\partial^2 u}{\partial x_3^2} + (c_L^2 - c_T^2) \frac{\partial^2 v}{\partial x_1 \partial x_3} = \frac{\partial^2 u}{\partial t^2}, \quad (55)$$

$$c_L^2 \frac{\partial^2 v}{\partial x_1^2} + c_T^2 \frac{\partial^2 v}{\partial x_3^2} + (c_L^2 - c_T^2) \frac{\partial^2 u}{\partial x_1 \partial x_3} = \frac{\partial^2 v}{\partial t^2}. \quad (56)$$

In Eq. (55) and Eq. (56), c_L and c_T are the phase velocities of longitudinal and shear waves, respectively.

It is convenient to formulate the problem in non-dimensional form. To this end, the displacement components are normalized with respect to the amplitude of the incident wave, A_{in} : $U = u/A_{in}$, $V = v/A_{in}$; the coordinates are rescaled with respect to the wavenumber of the longitudinal wave, k_L : $x_i = X_i/k_L$, and time is normalized by ω : $t = \tau/\omega$. Then, Eq. (55) and Eq. (56) become

$$\frac{\partial^2 U}{\partial X_1^2} + \frac{1}{\kappa^2} \frac{\partial^2 U}{\partial X_3^2} + \left(1 - \frac{1}{\kappa^2}\right) \frac{\partial^2 V}{\partial X_1 \partial X_3} = \frac{\partial^2 U}{\partial \tau^2}, \quad (57)$$

$$\frac{\partial^2 V}{\partial X_1^2} + \frac{1}{\kappa^2} \frac{\partial^2 V}{\partial X_3^2} + \left(1 - \frac{1}{\kappa^2}\right) \frac{\partial^2 U}{\partial X_1 \partial X_3} = \frac{\partial^2 V}{\partial \tau^2}, \quad (58)$$

in which $\kappa = c_L/c_T$.

The boundary conditions are also similarly transformed, and, in particular, Eq. (53.b) and Eq. (54.b) become

$$\kappa^2 \frac{\partial U^+}{\partial X_1} + (\kappa^2 - 2) \frac{\partial V^+}{\partial X_3} = \bar{K}_N (1 - \varepsilon \Delta U) \Delta U, \quad 0 \leq X_3 < D \quad (59)$$

$$\frac{\partial U^+}{\partial X_3} + \frac{\partial V^+}{\partial X_1} = \bar{K}_T (1 - \varepsilon \Delta U) \Delta V, \quad 0 \leq X_3 < D \quad (60)$$

respectively, where $D = k_L d$. In the latter equations, U^+ and V^+ are the normalized total displacement components on the positive side of the crack, while $\bar{K}_N = K_{N,0}/(k_L \mu)$ and $\bar{K}_T = K_{T,0}/(k_L \mu)$ are the normalized normal and tangential interfacial stiffness. The symbol μ represents the shear modulus of the medium. Finally, $\varepsilon = (K_{N,1}/K_{N,0})A_{in} = (K_{T,1}/K_{T,0})A_{in}$ measures the relative variation of the normal and of the tangential interfacial stiffness due to a change of the normal interface opening displacement equal to the amplitude of the incident wave. Note that the proportionality between ε and A_{in} implies that between the amplitude of the actual scattered second harmonic and A_{in}^2 . The magnitude of ε can be shown to be a monotonically decreasing function of the normalized interfacial stiffness, being always much smaller than one, except for interfaces which are nearly open, for which it tends to diverge. In this work, the dependence of ε on the normalized interface stiffness \bar{K}_N is that shown in Fig. 2 for Interface 1 and an incident longitudinal wave with an amplitude $A_{in} = 3$ nm. Thanks to this behavior of the nonlinear parameter ε , perturbation theory can be used to search for an approximate solution of the problem for nearly all the physically attainable interface conditions. Thus, solutions of the normalized equations of motion are sought in terms of power series of the small parameter ε ,

$$U(\overset{r}{X}, \tau) = U_0(\overset{i}{X}, \tau) + \varepsilon U_1(\overset{i}{X}, \tau) + \dots, \quad (61)$$

$$V(\overset{r}{X}, \tau) = V_0(\overset{i}{X}, \tau) + \varepsilon V_1(\overset{i}{X}, \tau) + \dots, \quad (62)$$

the terms proportional to ε or its powers playing the role of small corrections to U_0 and V_0 . By introducing the power series for U and V in the boundary conditions associated to the problem, and regrouping the terms which contain the same power of ε , a hierarchy of sets of boundary conditions for U_m and V_m , $m = 0, 1, \dots$ is obtained. In particular, the boundary conditions derived from Eq. (63.a-c) for the solutions of the symmetric zero-th order problem are found to be

$$\frac{\partial U_0^+}{\partial X_3} + \frac{\partial V_0^+}{\partial X_1} = 0, \quad X_1 = 0, 0 \leq X_3 < \infty, \quad (63.a)$$

$$\kappa^2 \frac{\partial U_0^+}{\partial X_1} + (\kappa^2 - 2) \frac{\partial V_0^+}{\partial X_3} = \bar{K}_N \Delta U_0, \quad 0 \leq X_3 < D, \quad (63.b)$$

$$U_0 = 0, \quad D \leq X_3 < \infty, \quad (63.c)$$

while those for the antisymmetric one are

$$\kappa^2 \frac{\partial U_0^+}{\partial X_1} + (\kappa^2 - 2) \frac{\partial V_0^+}{\partial X_3} = 0, \quad X_1 = 0, 0 \leq X_3 < \infty, \quad (64.a)$$

$$\frac{\partial U_0^+}{\partial X_3} + \frac{\partial V_0^+}{\partial X_1} = \bar{K}_T \Delta V_0, \quad 0 \leq X_3 < D, \quad (64.b)$$

$$V_0 = 0, \quad D \leq X_3 < \infty. \quad (64.c)$$

Similarly, those for the symmetric first-order problem are

$$\frac{\partial U_1^+}{\partial X_3} + \frac{\partial V_1^+}{\partial X_1} = 0, \quad X_l = 0, 0 \leq X_3 < \infty, \quad (65.a)$$

$$\kappa^2 \frac{\partial U_1^+}{\partial X_1} + (\kappa^2 - 2) \frac{\partial V_1^+}{\partial X_3} = \bar{K}_N \Delta U_1 - \bar{K}_N \Delta U_0^2, \quad 0 \leq X_3 < D, \quad (65.b)$$

$$U_1 = 0, \quad D \leq X_3 < \infty, \quad (65.c)$$

while the boundary conditions for the antisymmetric problem are

$$\kappa^2 \frac{\partial U_1^+}{\partial X_1} + (\kappa^2 - 2) \frac{\partial V_1^+}{\partial X_3} = 0, \quad X_l = 0, 0 \leq X_3 < \infty, \quad (66.a)$$

$$\frac{\partial U_1^+}{\partial X_3} + \frac{\partial V_1^+}{\partial X_1} = \bar{K}_T \Delta V_1 - \bar{K}_T \Delta V_0 \Delta U_0, \quad 0 \leq X_3 < D, \quad (66.b)$$

$$V_1 = 0, \quad D \leq X_3 < \infty. \quad (66.c)$$

Note the terms $\bar{K}_N \Delta U_0^2$ in Eq. (65.b) and $\bar{K}_T \Delta V_0 \Delta U_0$ Eq. (66.b) which play the role the incident field has in the zero-th order problem. Being products of solutions of the latter problem, in addition to time independent terms that are of no importance in this investigation, they contain contributions having a frequency that is twice that of the incident wave. Indeed, the solutions of the equations of motion having the same period of normalized incident wave, $T = 2\pi$, can be expressed as Fourier series over all the higher harmonics of the fundamental,

$$U(\overset{\Gamma}{X}, \tau) = \sum_{m=-\infty}^{+\infty} U(\overset{\Gamma}{X}|m) \exp(-jm\tau), \quad (67)$$

$$V(\overset{\Gamma}{X}, \tau) = \sum_{m=-\infty}^{+\infty} V(\overset{\Gamma}{X}|m) \exp(-jm\tau), \quad (68)$$

where $m \neq 0$, $\overset{\Gamma}{X} = (X_1, X_3)$, and $U(\overset{\Gamma}{X}|m)$ and $V(\overset{\Gamma}{X}|m)$ are the solutions of the coupled linear differential equations,

$$\frac{\partial^2 U}{\partial X_1^2} + \frac{1}{\kappa^2} \frac{\partial^2 U}{\partial X_3^2} + \left(1 - \frac{1}{\kappa^2}\right) \frac{\partial^2 V}{\partial X_1 \partial X_3} = -m^2 U, \quad (69)$$

$$\frac{\partial^2 V}{\partial X_1^2} + \frac{1}{\kappa^2} \frac{\partial^2 V}{\partial X_3^2} + \left(1 - \frac{1}{\kappa^2}\right) \frac{\partial^2 U}{\partial X_1 \partial X_3} = -m^2 V. \quad (70)$$

The solutions of these equations for the symmetric problem can be expressed as follows,

$$U^s(\overset{\Gamma}{X}|m) = \frac{2}{\pi} \int_0^\infty (\zeta A_m^s e^{-m\alpha_L X_3} - 2\kappa^{-2} \alpha_T C_m^s e^{-m\alpha_T X_3}) \sin(m\zeta X_1) d\zeta + \frac{2}{\pi} \int_0^\infty (\alpha_L B_m^s e^{-m\alpha_L X_1} + 2\kappa^{-2} \zeta D_m^s e^{-m\alpha_T X_1}) \cos(m\zeta X_3) d\zeta, \quad (71)$$

$$\begin{aligned}
V^s(\bar{X}|m) &= \frac{2}{\pi} \int_0^\infty (\alpha_L A_m^s e^{-m\alpha_L X_3} - 2\kappa^{-2} \zeta C_m^s e^{-m\alpha_T X_3}) \cos(m\zeta X_1) d\zeta + \\
&\quad \frac{2}{\pi} \int_0^\infty (\zeta B_m^s e^{-m\alpha_L X_1} + 2\kappa^{-2} \alpha_T D_m^s e^{-m\alpha_T X_1}) \sin(m\zeta X_3) d\zeta
\end{aligned} \tag{72}$$

while those of the antisymmetric problem are

$$\begin{aligned}
U^a(\bar{X}|m) &= \frac{2}{\pi} \int_0^\infty (\zeta A_m^a e^{-m\alpha_L X_3} - 2\kappa^{-2} \alpha_T C_m^a e^{-m\alpha_T X_3}) \cos(m\zeta X_1) d\zeta + \\
&\quad \frac{2}{\pi} \int_0^\infty (\alpha_L B_m^a e^{-m\alpha_L X_1} + 2\kappa^{-2} \zeta D_m^a e^{-m\alpha_T X_1}) \sin(m\zeta X_3) d\zeta
\end{aligned} \tag{73}$$

$$\begin{aligned}
V^a(\bar{X}|m) &= \frac{2}{\pi} \int_0^\infty (-\alpha_L A_m^a e^{-m\alpha_L X_3} + 2\kappa^{-2} \zeta C_m^a e^{-m\alpha_T X_3}) \sin(m\zeta X_1) d\zeta - \\
&\quad \frac{2}{\pi} \int_0^\infty (\zeta B_m^a e^{-m\alpha_L X_1} + 2\kappa^{-2} \alpha_T D_m^a e^{-m\alpha_T X_1}) \cos(m\zeta X_3) d\zeta
\end{aligned} \tag{74}$$

In Eq. (71) to (74), $A_m^{s,a}$, $B_m^{s,a}$, $C_m^{s,a}$, $D_m^{s,a}$ are unknown functions of ζ to be determined by enforcing the appropriate boundary conditions, and α_L and α_T , are defined on the real axis so that

$$\alpha_L = \begin{cases} \sqrt{\zeta^2 - 1}, & \text{if } \zeta \geq 1 \\ -j\sqrt{1 - \zeta^2}, & \text{if } \zeta < 1 \end{cases}, \text{ and } \alpha_T = \begin{cases} \sqrt{\zeta^2 - \kappa^2}, & \text{if } \zeta \geq \kappa \\ -j\sqrt{\kappa^2 - \zeta^2}, & \text{if } \zeta < \kappa \end{cases}.$$

The total components of the normalized displacement fields are recovered from the solution of the symmetric and antisymmetric problems according to the following rules:

$$\begin{aligned}
U(X_1, X_3) &= U^s(X_1, X_3) + U^a(X_1, X_3), & \text{for } X_1 > 0, \\
U(|X_1|, X_3) &= -U^s(|X_1|, X_3) + U^a(|X_1|, X_3), & \text{for } X_1 < 0, \\
V(X_1, X_3) &= V^s(X_1, X_3) + V^a(X_1, X_3), & \text{for } X_1 > 0, \\
V(|X_1|, X_3) &= V^s(|X_1|, X_3) - V^a(|X_1|, X_3), & \text{for } X_1 < 0.
\end{aligned}$$

The details of the mathematical procedure to solve these problems were reported in the work of Achenbach *et al.* (1980) and Mendelsohn *et al.* (1980), and will not be repeated here. The only relevant addition to that treatment is the explicit and repeated use of the harmonic balance method to match the time-dependence of the scattered field with that of the driving terms given either by the incident field in boundary conditions for the zero-th order problems, or by the products of the zero-th order components in Eq. (65.b) and Eq. (66.b). The solutions of the zero-th order problem, thus, can be shown to contain only contributions with the same frequency as the incident field, while those of the first-order system, disregarding a constant term of no interest for the present investigation, describe scattered fields with frequency twice as that of the incident wave.

2.4.3 Numerical results

Several are the parameters which determine the dynamics of an interface between two rough surfaces in contact, and even more those which are required to describe the nonlinear scattering of an acoustic wave from a surface-breaking crack with faces in partial contact. As an exhaustive parametric study would go beyond the scope of the present work, the focus of the latter is set only on those parameters which most notably affect the detection and localization of the nonlinear defect of interest here. Both shear vertical (SV) and Rayleigh wave incidence are considered next. The frequency of the incident wave is set to be $f = 5$ MHz.

2.4.3.1 Shear vertical incidence

SV waves are commonly used for the nondestructive inspection of components in nuclear power plants and in the railway industry. Searching for cracks breaking the surface opposite that on which the transmitter is placed, such waves are often sent into the component along a direction of propagation which forms an angle of 45 degrees with the normal to the surface.

Given the importance of SV waves as a probing tool for surface-breaking cracks, this investigation starts by considering the effect of the angle of incidence, θ_{in} , of such a mode on the acoustic response of a partially closed, surface-breaking crack. The angle of incidence is measured from the x_3 axis, that is to say, from the plane containing the crack. The incident wave is assumed to propagate from infinity towards the stress-free surface with a propagation vector k_T . In all the following simulations, the dependence of the nonlinear parameter ε on the interface stiffness is that shown in Figure 2, and the amplitude of the incident wave, A_{in} , is equal to 3 nm.

Figures 13 and 14 show the dependence on the angle of incidence, θ_{in} , of the horizontal components of the linear and nonlinear backscattered total field, respectively, at increasing depth within the bulk of the material. A similar behavior is displayed by the vertical components. Note that in these and all the subsequent figures the following notation convention has been used: $U(\dot{X} | m) = U_m(\dot{X})$, and $V(\dot{X} | m) = V_m(\dot{X})$. The most relevant feature of these plots is the marked peak around the critical angle of the longitudinal wave, θ_L . This finding can be easily explained by considering that, just above θ_L , the amplitude of the reflected longitudinal wave reaches values nearly 2.5 times higher than that of the incident wave. Furthermore, in the neighborhood of θ_L the dominant component of the total incident field is σ_{11} , which, more efficiently than any other, excites the normal vibration mode of the crack. Worthy of notice, because contrary to the assumptions underlying the method most commonly employed to search for surface-breaking cracks, is also the considerably smaller response around 45 degrees angle of incidence.

The effect of the crack's depth on the modulus of the normalized horizontal and vertical displacement components is illustrated in Fig. 15 for the first harmonic wave and in Fig. 16 for the second harmonic. The angle of incidence of the incident SV wave is equal to 34 degrees, the normalized interface stiffness and the nonlinear parameter are $\bar{K}_N = 1.95$ and $\varepsilon = 0.144$, respectively. The observation point is placed along the

direction of propagation of the incident wave at a normalized distance $R = k_L r = 30$ from the crack's mouth, where r indicates the actual distance. An initial monotonic increase of both linear components is predicted up to a value of D of the order of 1.5, after which they remain at the same level for values of D up to 2. The latter value corresponds to an actual crack's depth of four wavelengths of the incident shear wave. The nonlinear components, on the other hand, reach their maximum values around $D = 1$, after which they tend to decrease. Deeper cracks are expected to produce linear and nonlinear components having modulus within the ranges shown in Fig 15 and Fig. 16, respectively.

The magnitude of the nonlinear response predicted by the model and presented in these examples is large enough that some doubt may be cast on the accuracy of a first-order approximation. However, a closer examination of the results show that for smaller values of ε corresponding to closer cracks, and at angles of incidence not too close to the critical angle of the longitudinal waves, the magnitude of the second harmonic field generated upon scattering is well within the range of values where the perturbation approach provides accurate results. To illustrate this point, Figure 17 shows the dependence of the ratio between the absolute values of the horizontal displacement of the scattered second and first harmonic components on the normalized crack dimension, D , for two typical values of θ_{in} , 45 and 60 degrees, as well as for 34 degrees. The observation point is again at a distance $R = 30$, and the normalized interface stiffness and nonlinear parameter are those of Figures 15 and 16. The second harmonic's response at 45 is always more than 10 dB below that at 34 degree incidence for all values of the normalized crack depth. Similarly, the response at 60 degrees remains considerably below that at 34 degree incidence for values of $D < 1$, although it approaches the latter for $D > 1$. The conclusion to draw from this figure is that, not only the absolute levels of the linear and nonlinear backscattered fields are higher at 34 degree of incidence than at any other angle of incidence, but also the efficiency of the second harmonic generation is the highest for angles of incidence just above θ_L , especially for cracks with depth $D < 1$.

Next, the variation of the modulus of the Cartesian components of the backscattered displacement field with the distance from the crack is considered for a shear wave incident at 34 degrees. The observation point moves along the direction of propagation of the incident wave. The normalized depth of the crack is $D = 0.5$, which is approximately equal to one wavelength of the shear wave, while the normalized interface stiffness $\bar{K}_N = 1.95$ and the nonlinear parameter $\varepsilon = 0.144$. Figure 18 illustrates the dependence of the scattered first harmonic, and Fig. 19 that of the second one on the distance of the observation point from the crack's mouth, R . The horizontal component of both harmonics show a rapid decay to occur within a distance equal to 2 from the crack's mouth, while the vertical components tends to decay more slowly.

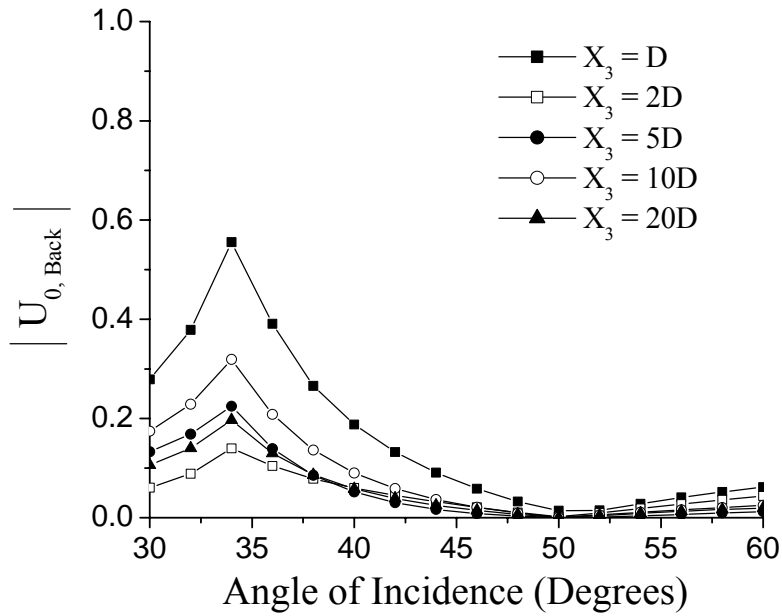


Figure 13. Normalized backscattered horizontal displacement of the linear field versus the angle of incidence for increasing values of the normalized depth of the observation point. The latter is measured in terms of normalized crack's depth, D . The normalized crack's depth is $D = 0.5$, while $\bar{K}_N = 1.95$ and $\varepsilon = 0.144$.

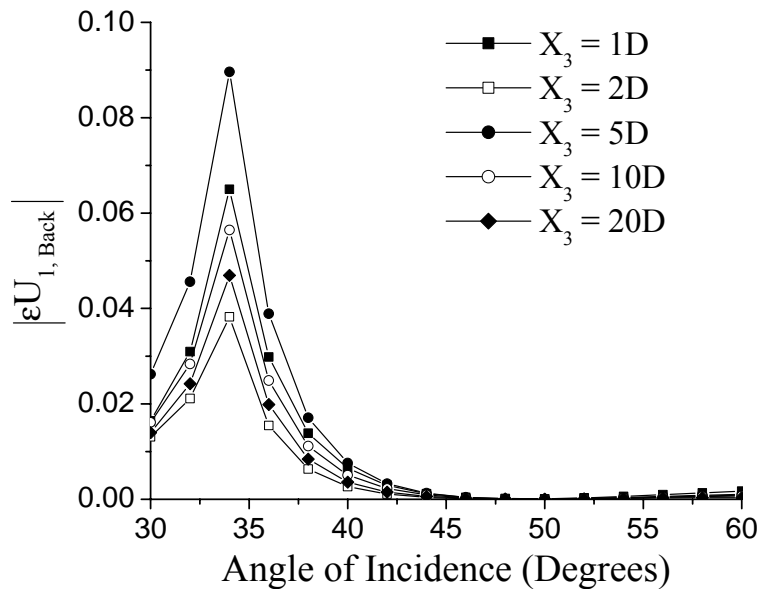


Figure 14. Normalized backscattered horizontal displacement of the nonlinear field versus the angle of incidence for increasing values of the normalized depth of the observation point. The latter is measured in terms of normalized crack's depth, D . The normalized crack's depth is $D = 0.5$, while $\bar{K}_N = 1.95$ and $\varepsilon = 0.144$.

Such a behavior may be understood in terms of the increasing constraining effect of the surrounding material on the motion of the particles as the observation point moves away from both the crack's and half-space's surface.

Figure 20 shows the variation of the modulus of εU_I and εV_I with the interface closure, i.e., for increasing values of the normalized interface stiffness \bar{K}_N . The observation point is placed along the backscattering direction at a normalized distance $R = 30$ from the crack's mouth. The normalized crack depth is $D = 0.5$. After an initial dramatic increase corresponding to the formation of first contacts, the moduli of the Cartesian nonlinear components decay in a monotonic fashion which strongly resembles that predicted for the nonlinear response on an infinite interface.

In the Introduction, results obtained by Krohn *et al.* (2002) were reported for their relevance on the issue of defect location by means of nonlinear ultrasonic techniques. In particular, it was mentioned that using laser interferometric detection, a highly localized nonlinear response of delaminations could be detected within the composite plate. It was also reported that, so far, no convincing explanation for such a strong localization has been given, although some form of trapping mechanism of the energy carried by the generated second harmonic wave by the delamination itself has been hypothesized (Solodov, 2003). Although apparently simplistic, two remarks are in order. The first one concerns the detection technique, which is sensitive to the displacement component normal to the inspected surface. The second remark regards the fact that the delamination is likely to be roughly parallel to the surface on which the measurements are carried out. Therefore, considering that in the experiments mentioned above the wavelength of the acoustic excitation is much larger than the plate thickness, it is reasonable to conceive that the behavior of the normal component of the displacement of the higher harmonic wave detected at the stress-free surface closely resembles that at the crack's location. Figure 21 illustrates the dependence of the εU_I component, that is to say, the second harmonic component of the crack's normal vibration, on the coordinate X_3 at $X_1 = 0^-$, that is to say, along the plane containing the crack. The crack's normalized depth is $D = 0.5$, the normalized interface stiffness and nonlinear parameter are $\bar{K}_N = 1.95$ and $\varepsilon = 0.144$. A sudden drop of the modulus of εU_I is observed at the crack tip, which exceeds 30 dB. This prediction of the model supports the interpretation of the highly localized nonlinear response of a delamination in a composite plate as due to the fact that the technique used under the circumstances described above monitors the nonlinear component of normal opening displacement of the delamination.

Finally, it should be remarked that, for all the cases considered so far, very similar theoretical results have been obtained for the same field variables in the forward scattering direction, and, for this reason, they have not been presented here.

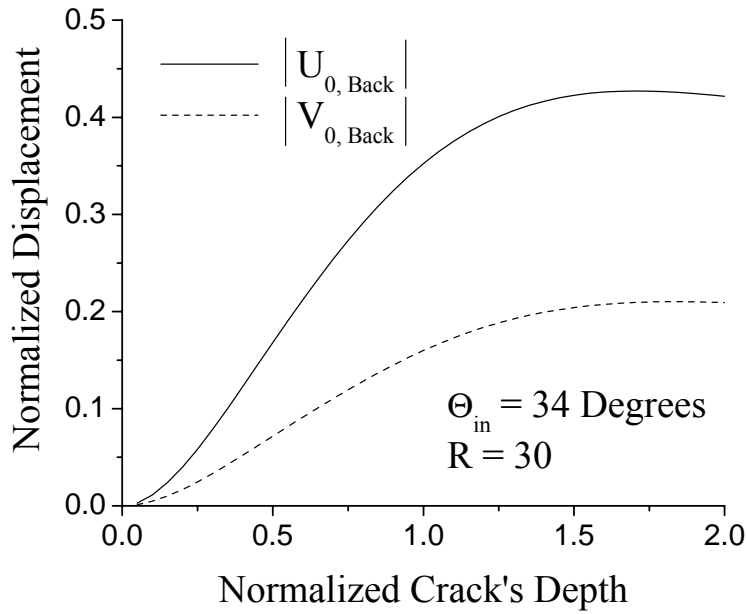


Figure 15. Normalized backscattered components of the linear displacement as a function of the normalized crack's depth. The angle on incidence is equal to 34 degrees, and the observation point is at a normalized distance, R , equal to 30 from the crack's mouth along the propagation direction of the incident wave. Also, $\bar{K}_N = 1.95$ and $\varepsilon = 0.144$.

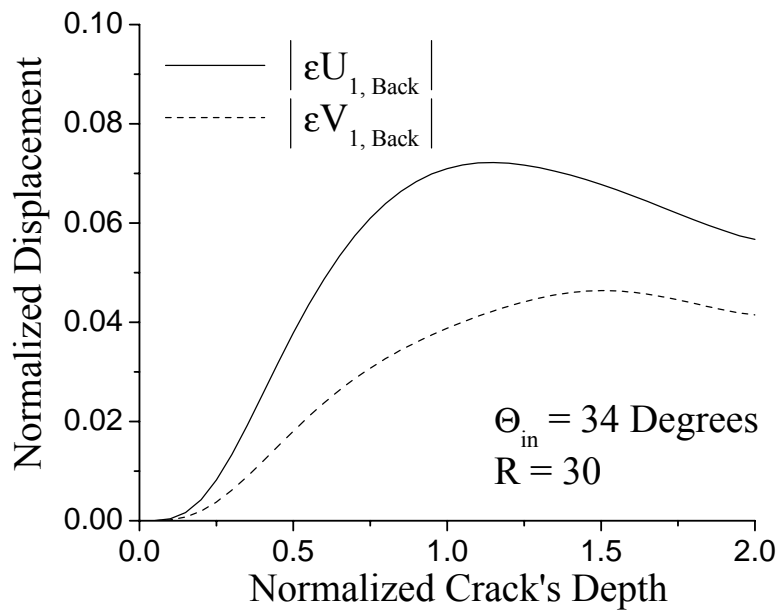


Figure 16. Normalized backscattered components of the nonlinear displacement as a function of the normalized crack's depth. The angle on incidence is equal to 34 degrees, and the observation point is at a normalized distance, R , equal to 30 from the crack's mouth along the propagation direction of the incident wave. Also, $\bar{K}_N = 1.95$ and $\varepsilon = 0.144$.

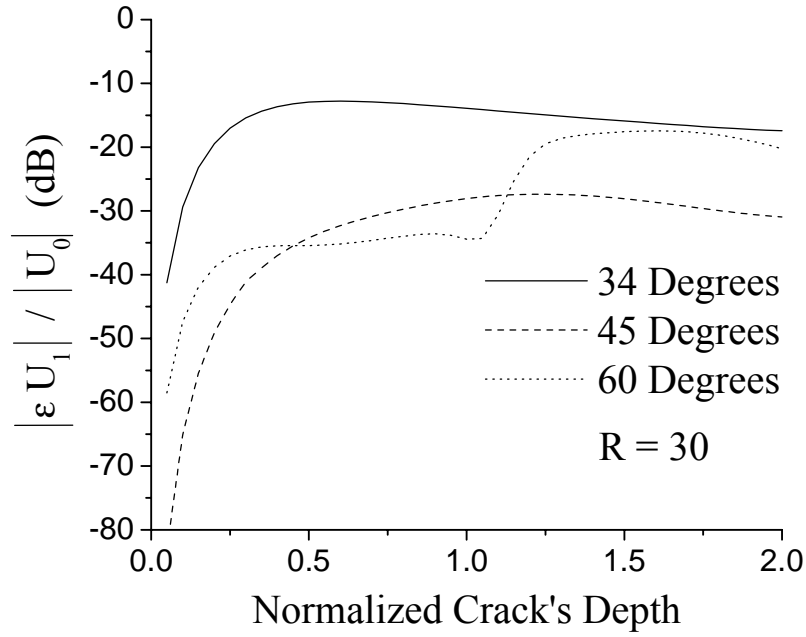


Figure 17. Variation of the backscattered second harmonic wave relative to the first harmonic versus the normalized crack's depth. The parameters defining the system are those of the previous two figures.

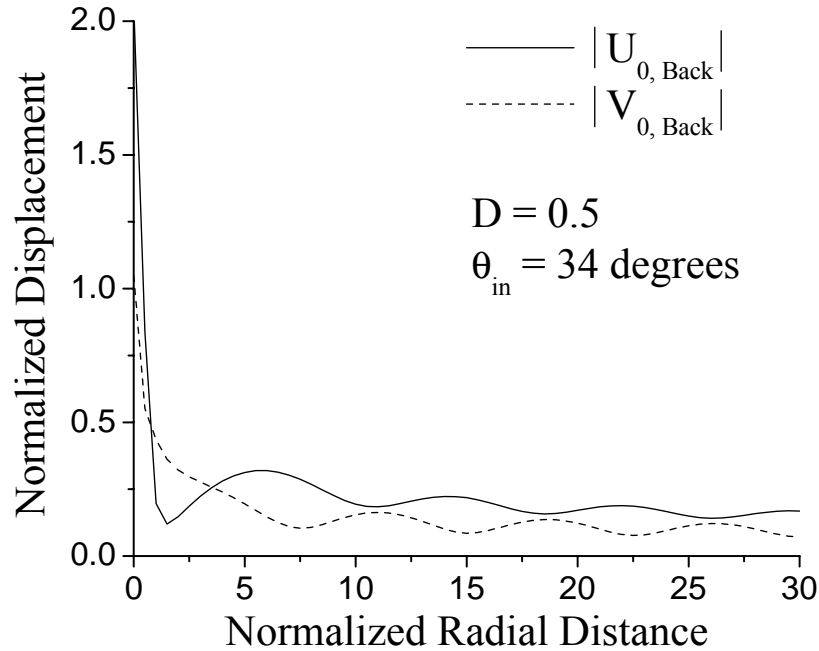


Figure 18. Normalized backscattered components of the linear field versus distance from the crack's mouth. The observation point is placed along the propagation direction of the incident wave, i.e., $\theta_{in} = 34$ degrees. The normalized crack's depth is $D = 0.5$, $\bar{K}_N = 1.95$, and $\varepsilon = 0.144$.

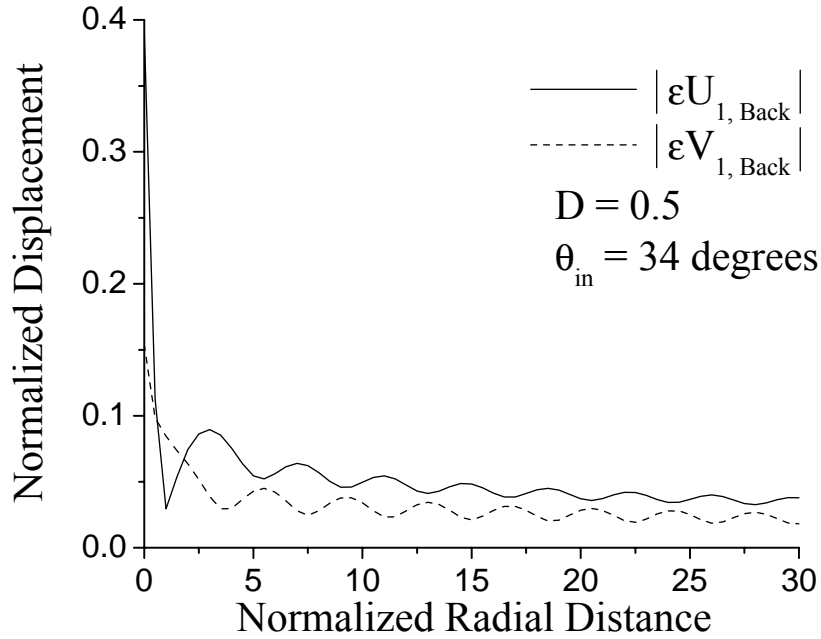


Figure 19. Normalized backscattered components of the nonlinear field versus distance from the crack's mouth. The observation point is placed along the propagation direction of the incident wave, i.e., $\theta_{in} = 34$ degrees. The normalized crack's depth is $D = 0.5$, $\bar{K}_N = 1.95$, and $\varepsilon = 0.144$.

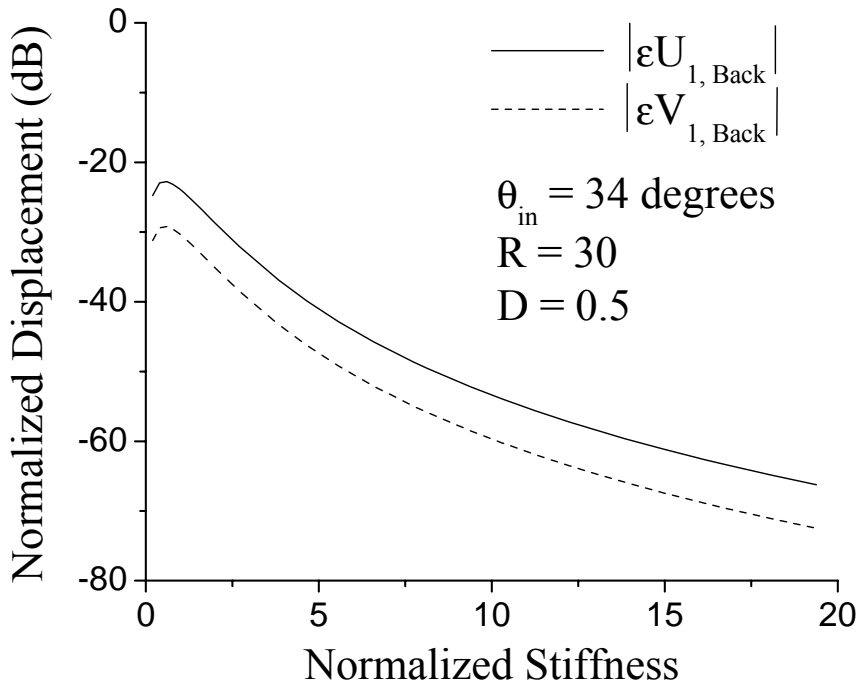


Figure 20. Normalized backscattered horizontal component of the nonlinear displacement field versus the normalized interfacial stiffness. The normalized distance of the observation point is $R = 30$. The remaining system parameters are those of the preceding figure.

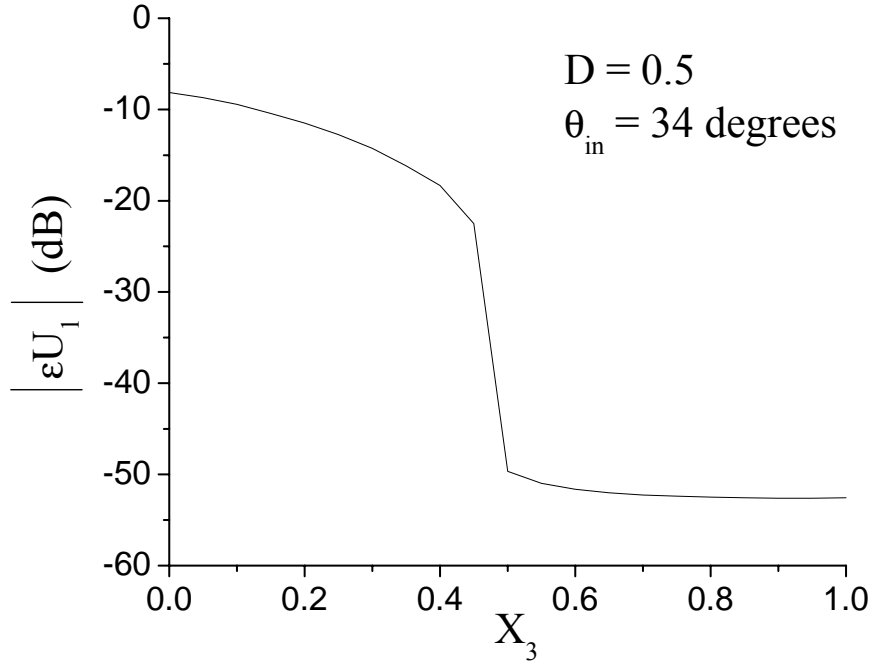


Figure 21. Dependence of the normalized nonlinear component of the displacement normal to the crack on X_3 for $X_1 = 0$. The system parameters are those of Figure 19.

2.4.3.2 Rayleigh wave incidence

The case of a Rayleigh wave insonifying a partially closed surface-breaking crack is considered next. The amplitude of the horizontal displacement component of the incident wave at the stress-free surface is chosen to be equal to 3 nm: $u_{in}(x_1, x_3 = 0) = 3$ nm.

Figure 22 illustrates the behavior of the modulus of the second harmonic component of the horizontal displacement at four values of the depth, X_3 , as a function of the variable X_1 . The first harmonic component's dependence displays features similar to those of the second harmonic, and, therefore, is not shown here. The normalized crack's depth is $D = 0.5$, and the interfacial stiffness and nonlinear parameter are again $\bar{K}_N = 1.95$ and $\varepsilon = 0.144$. As in the case of SV incidence, in the plane $X_1 = 0$ the displacement component normal to the crack's plane undergoes a dramatic and sudden drop at the tip of the crack. The forward scattered second harmonic wave is also shown to approach an average value slightly higher than that of the backward scattered component as the value of X_1 increases in both directions.

The effect of the interface closure on the modulus of both vertical and horizontal second harmonic components of the displacement field is illustrated in Fig. 23. The observation point is placed at the surface of the half-space, at a distance $X_1 = -30$ from the crack's mouth. The general features of the displayed behavior are those already seen in Fig. 20, except for the level of the signal which is about 10 dB higher in the case

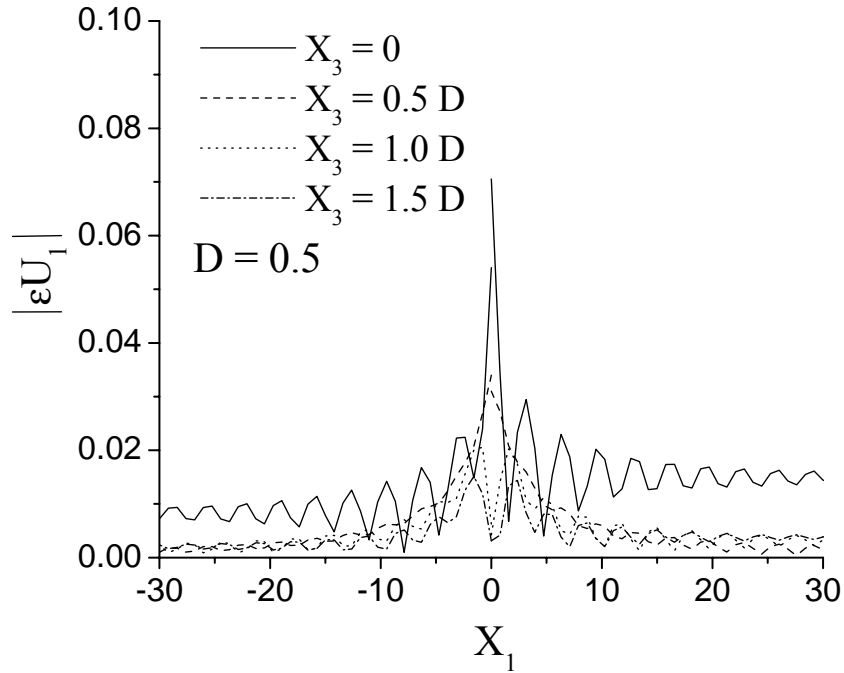


Figure 22. Normalized backscattered horizontal displacement of the nonlinear field versus X_1 at four different values of X_3 . The latter is measured in terms of normalized crack's depth, D . The normalized crack's depth is $D = 0.5$, while $\bar{K}_N = 1.95$ and $\varepsilon = 0.144$.

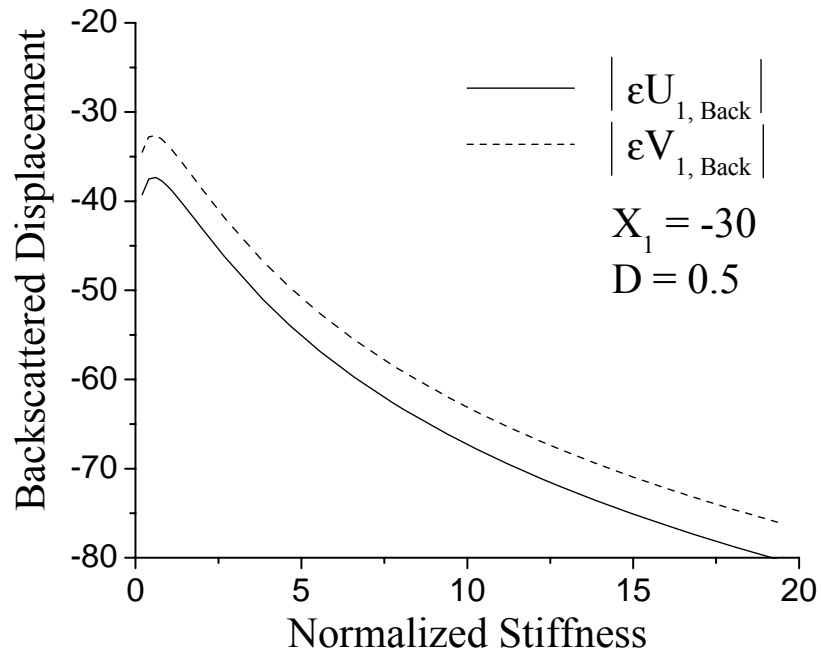


Figure 23. Normalized backscattered horizontal component of the nonlinear displacement field versus the normalized interfacial stiffness. The observation point is placed on the surface of the half-space at a normalized distance $X_1 = -30$. The remaining system parameters are those of the preceding figure.

of a SV wave backscattered at 34 degrees, that is to say, at an angle just above the critical angle for the longitudinal wave.

Finally, Fig. 24 and Fig. 25 show the backward and forward normalized Cartesian components of the nonlinear scattered field at a distance $|X_1| = 30$ on the surface of the half-space as functions of the normalized crack's depth, D . The values of the interfacial stiffness and of the nonlinear parameter are those already used in Fig. 22. A remarkable and surprising difference of behavior between the forward and the backward can be easily noticed, as the former increases nearly monotonically with the crack's depth up to $D \approx 1$ to remain roughly at the same level afterwards, while the latter displays pronounced interference features for values of $D < 1$. To be registered is also the considerably higher values of the forward scattered field compared to that scattered in the opposite direction.

2.4.4 Summary and concluding remarks

A theoretical model which predicts the generation of the second harmonic component upon scattering of an incident harmonic wave by a surface-breaking crack with faces in partial contact has been presented. The cases of shear vertical and Rayleigh wave incidence have been considered, and for each, the effect of parameters such as the angle of incidence, the crack's depth, and crack's closure have been examined. The nonlinearity of the scattering defect has been introduced into the mathematical formulation of the problem by extending the boundary conditions at the crack's contacting faces to account for the effect of the two-dimensional distribution of elastic contacts. It has been found that the highest linear and nonlinear responses of such a defect occur when the latter is insonified by a shear vertical wave incident on the surface containing the crack at an angle which is just above the critical angle of the longitudinal wave, θ_L . Further, the generation of the second harmonic has been shown to be the most efficient in such a configuration. The relevance of this finding stems in part from the fact that the inspection methods currently used to search for surface-breaking cracks utilize SV wave at 45 degree incidence. As demonstrated in this work, at 45 degree incidence the sensitivity of an inspecting SV wave to such defects is much lower than that shown at 34 degrees. This problem is dealt with in further details in a manuscript under preparation.

An additional important advantage offered SV waves at 45 degree incidence concerns the localization of a defect. In fact, the exploitation of the efficient mode conversion of the incident SV wave into an evanescent longitudinal wave propagating along the surface renders this configuration considerably more sensitive to crack-like defects located at the surface of the sample than to any other defect placed along the direction of propagation of the incident field. Therefore, in search for surface-breaking cracks by means of nonlinear scattering techniques, the set-up providing the highest sensitivity also offers a solution to the localization problem. In this respect, an additional important result of this work has been the key to interpret recent experimental results by Krohn *et al.* (2002) showing a highly localized nonlinear response of delaminations in composite materials. In fact, the model indicates that the experimental observations capture the very rapid decay of the nonlinear opening displacement normal to the delamination beyond the borders of the latter. The model predicts a magnitude of

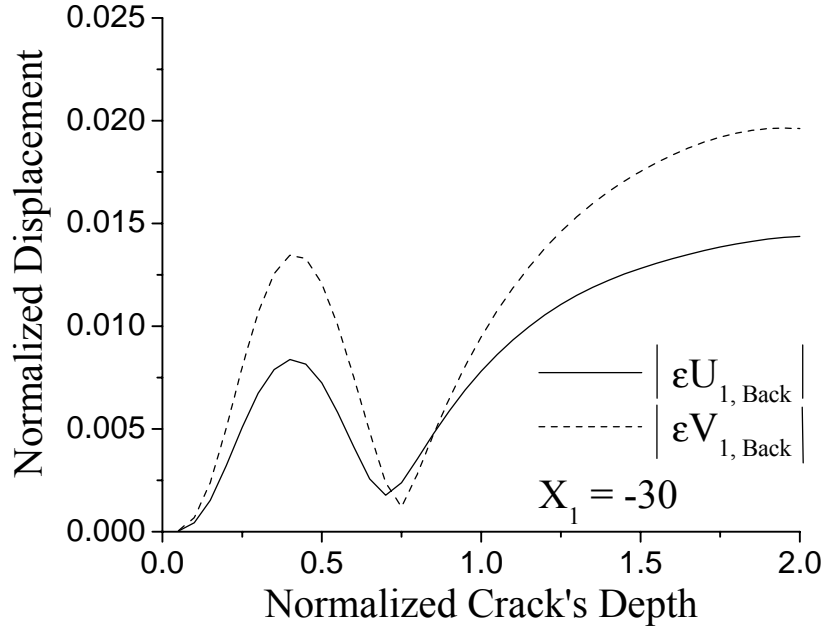


Figure 24. Normalized backscattered components of the nonlinear field versus the normalized crack's depth. The observation point is placed on the surface of the half-space at a normalized distance $X_1 = -30$. The normalized crack's depth is $D = 0.5$, $\bar{K}_N = 1.95$, and $\varepsilon = 0.144$.

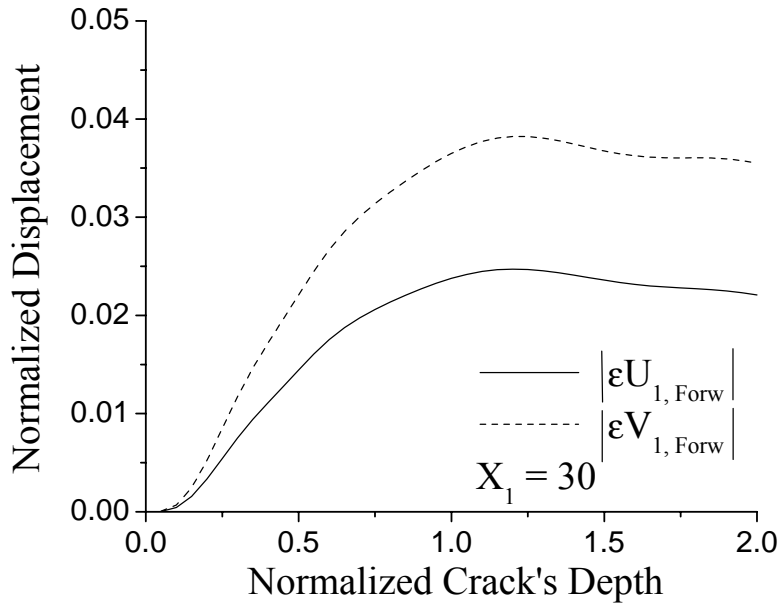


Figure 25. Normalized forward scattered components of the nonlinear field versus the normalized crack's depth. The observation point is placed on the surface of the half-space at a normalized distance $X_1 = 30$. The normalized crack's depth is $D = 0.5$, $\bar{K}_N = 1.95$, and $\varepsilon = 0.144$.

such a drop to be of the order or 30 dB, which exceeds the experimentally observed behavior by at least 10 dB. A possible reason for such an overestimation may be the

asymmetric position of the actual delamination within the plate's cross section. In fact, if located outside the mid plane of the plate, the crack is likely to generate a scattered field which cannot be decomposed into a symmetric and antisymmetric part, the former yielding a nearly null contribution to the component of the displacement field normal to the crack on the plane containing the latter (Eq. (15c)).

Finally, for both SV and Rayleigh incidence, the magnitude of the nonlinear response decays monotonically after reaching a maximum for values of the normalized stiffness around 1. Even in this case, however, the backscattered field generated upon scattering of a SV wave incident at angles slightly higher than θ_L is larger than that due to a Rayleigh wave.

3 Experimental investigation

3.1 Introduction

Serious delays in securing the funding for the acquisition of the instrumentation required to carry out the experimental program of this project are at the origin of the incompleteness of the tasks as described in the original proposal. Indeed, as planned in the original proposal, the experimental part of the project was expected to last about 20 months. On the other hand, laboratory test could start only eight months before the end of the project. Delays notwithstanding, significant progress have been marked in this period and the results which have been obtained provide a solid ground on which further research and development may be based.

The focus of the initial effort has been the optimization of the available experimental set-up with respect to the reduction of the spurious signals generated by the instrumentation. In particular, the abatement of the residual second harmonic to a level more than -60 dB below the component at the fundamental frequency has been achieved. This result has allowed the attainment of the results described in the following section.

3.2 Steel-steel interfaces: experimental results

Three steel blocks have been prepared with nominally flat surfaces having rms roughness (σ) values equal to 0.2 μm , 0.24 μm , and 0.3 μm , respectively. A fourth block (the 'Base' block in Figure 26) was especially designed to host the ultrasonic transducer and to allow the external pressure to be transmitted to the steel-steel interface under investigation without affecting the coupling between the transducer and sample. Two interfaces were constructed by combining two surfaces forming a composite one with roughness $\Sigma_1 = (\sigma_1^2 + \sigma_2^2)^{1/2} = 0.3 \mu\text{m}$, and $\Sigma_2 = (\sigma_1^2 + \sigma_3^2)^{1/2} = 0.38 \mu\text{m}$.

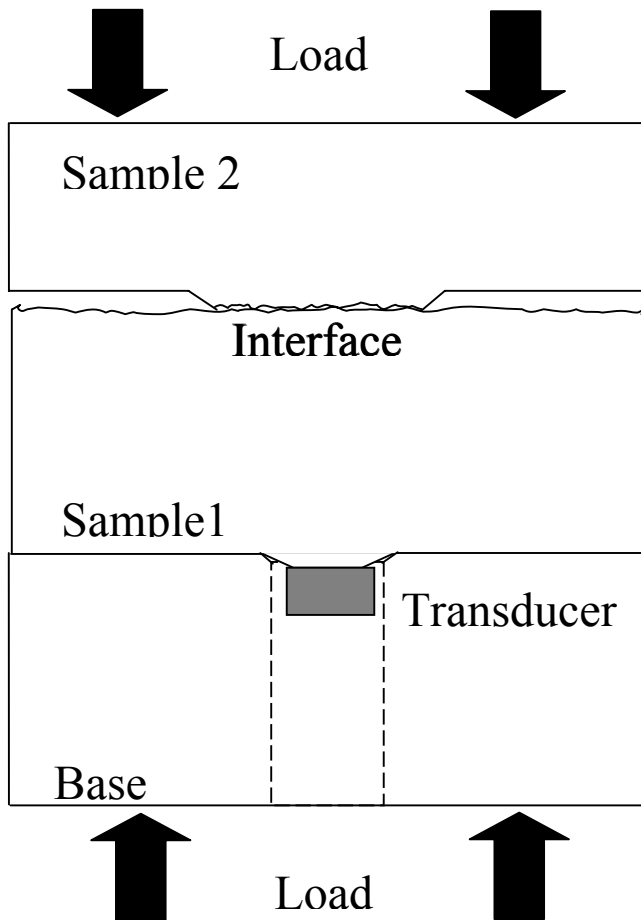


Figure 26. Schematic representation of the experimental set-up.

Cycles were run with maximum pressure reaching the value of 250 KNw, corresponding to a maximum nominal pressure of 200 MPa. Considering that the plastic deformation in steel is expected to begin at pressure values of that order of magnitude, and that the actual local stresses supported by the individual asperities in contact are indeed much higher than the nominal applied pressure, plasticity occurs in the asperities in contact, the effect of which is systematically observed in our experiments.

The measurements have been carried out in reflection mode, by using a broadband transducer (Panametrics, model V541) operating at 5 MHz both as a source as well as a receiver. The resonance frequency of the transducer was determined to be around 4.2 MHz. The use of a transducer with the first resonance occurring at 4.2 MHz reduces the sensitivity to the second harmonic component by well more than 20 dB, as it could be evaluated by comparing the signal's amplitude when the transducer was excited by a tone burst at 5 MHz and 10 MHz, respectively.

Figure 27 illustrates the behaviour of the first harmonic component reflected by the steel-steel interface with composite roughness $\Sigma = 0.3\mu\text{m}$ as a function of the applied pressure. The expected hysteresis caused by plasticity is observed during a single loading cycle. A theoretical model developed by Kim *et al.* (2004) explains the linear acoustic response of an elasto-plastic interface. The model points out two major differences with respect to the linear elastic case. The first major difference concerns the dynamic interface stiffness of the interface during the compressive phase of loading

cycle. At each value of the compressive load, the dynamic stiffness of an elasto-plastic interface during is the stiffness the interface displays during the initial phase of unloading from that particular point of the loading path. Note that the dynamic stiffness is always larger than the static stiffness. The second key feature of the dynamics of an elasto-plastic interface is its increased dynamic stiffness during unloading with respect to that displayed during compression. This feature is the consequence of the increased radius of curvature of the asperities in contact due to their plastic deformation during loading. The effect of such an increase of the interfaces dynamic stiffness is the lower reflectivity illustrated by the results of Fig. 27.

On the same interface of Figure 27 and during the same loading cycle, the generation of the second harmonic component was also recorded. Figure 28 reports the results. The nonlinear signal increases rapidly as the contacts are formed under the effect of the external pressure, reaching a plateau when the load approaches the value of about 20 KNw. During the remaining part of the loading cycle the signal appears to remain approximately at the same level, which is oscillate between 25 to 30 dB above the threshold of the noise.

The level of nonlinear harmonic generation has been observed to reach values up to 40 dB above noise with rough surfaces which have not previously plastically deformed.

Figure 29 reports data acquired on a second interface with rms $\Sigma = 0.38 \mu\text{m}$, which has been loaded to pressure values as high as 200 MPa. Even in this case, the amplitude of the second harmonic rapidly increases with the applied load, reaching a maximum value at 75 KNw, which is more than 20 dB above the noise, and decreases as predicted by the theoretical model presented earlier (see Figure 3). The relevance of these data, however, stems from the considerable nonlinear generation by the interface even at stress values that are comparable with the largest residual stresses measured in nuclear power components (Payzant *et al.* 1996). This observation supports our expectations that, *even for stress-corrosion cracks subjected to the largest residual stresses occurring in a weld, their nonlinear response is larger than the background noise.*

Finally, Figure 30 demonstrates the quadratic dependence of the amplitude of the second harmonic on the amplitude of the fundamental, as predicted by the theory (see Eq. 19 and related comments). The applied load is 50 KNw.

In conclusion, the experimental results acquired in this project show that *a considerable dynamic range is available for the detection of partially closed defects by means of nonlinear techniques that are sensitive to the generation of the second harmonic wave.*

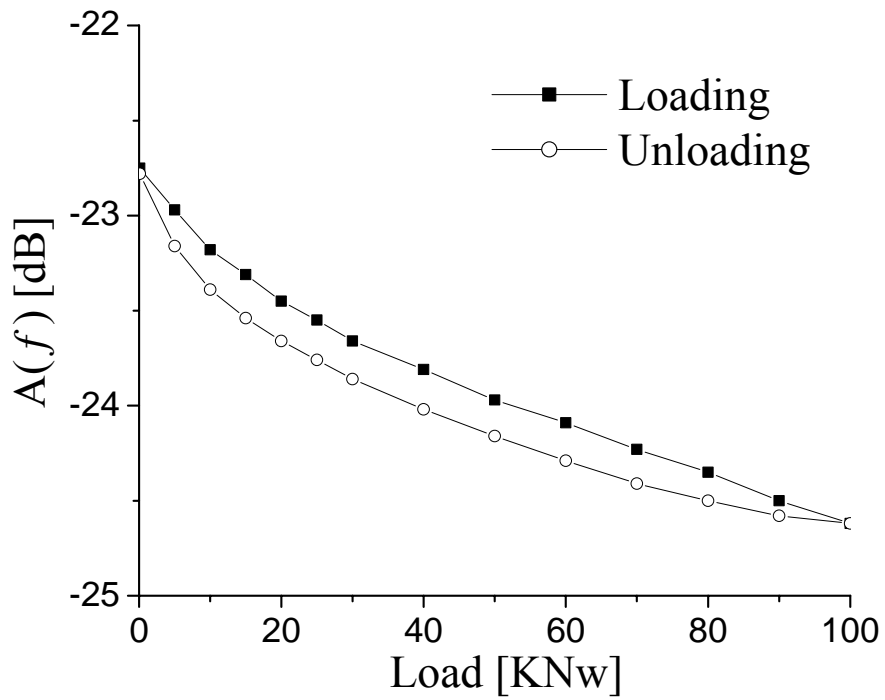


Figure 27. Amplitude of the first harmonic component reflected by the interface between two rough surfaces as a function of the applied load.

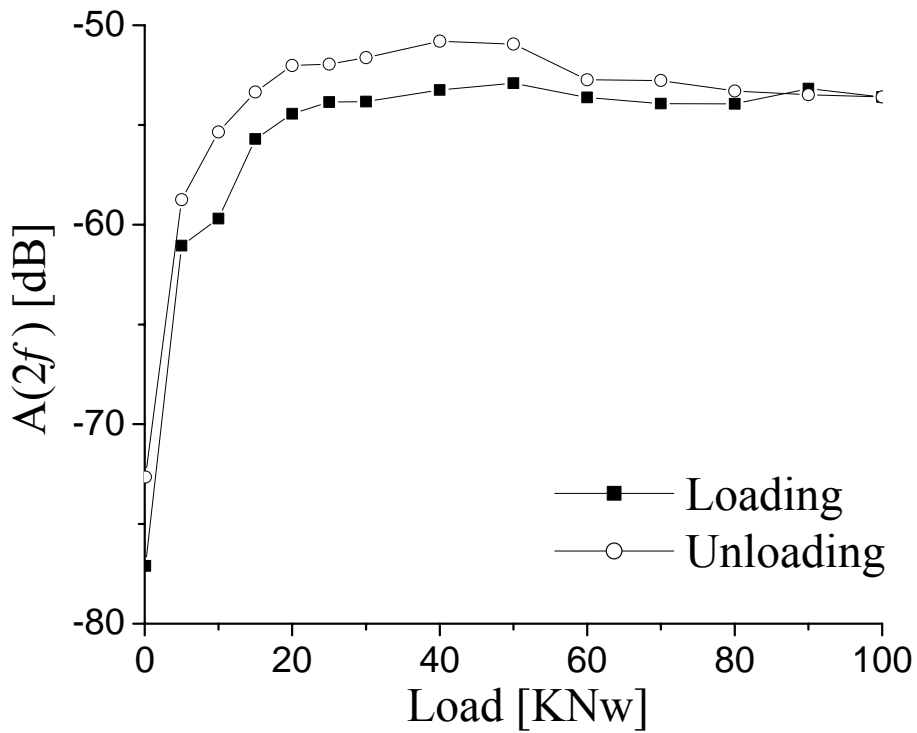


Figure 28. Second harmonic component generated by the same interface of Figure 27 versus the applied load.

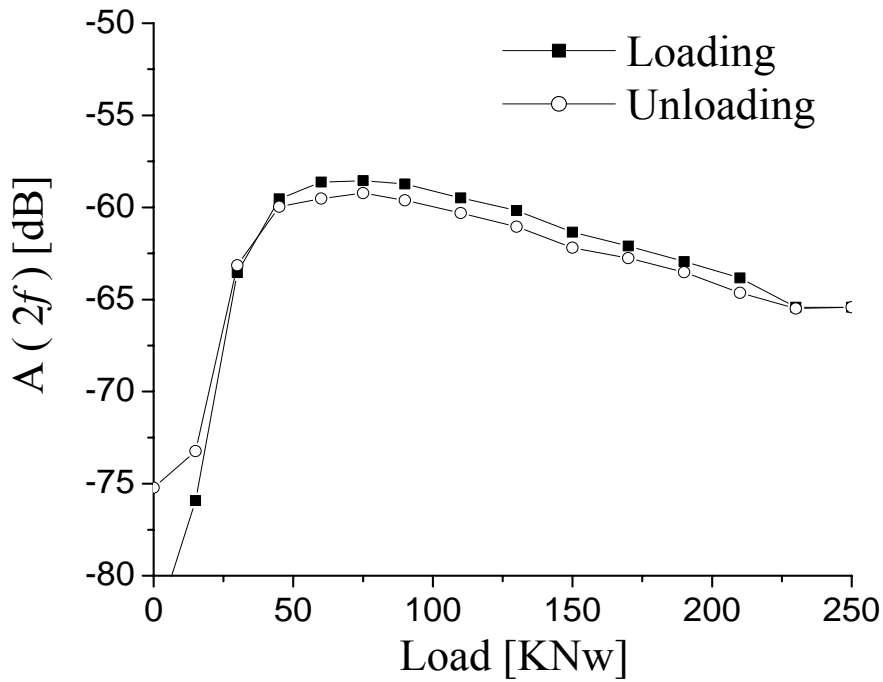


Figure 29. Second harmonic component generated by a steel-steel interface with a composite roughness $\Sigma = 0.38$ microns versus the applied load. The loading cycle reaches a maximum value of 200 MPa, which is comparable with the largest residual stresses observed in weld.

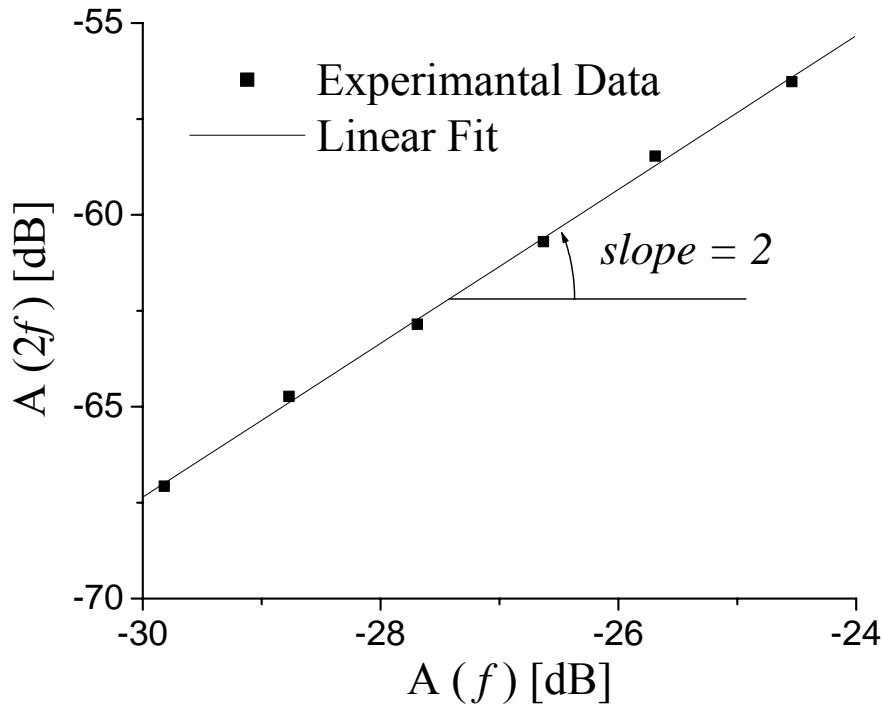


Figure 30. Amplitude of the second harmonic component versus that of the first one. The continuous line represent the best linear fit. The slope of the straight line is equal to 2, as predicted by the theory. The applied load is 50 KNw.

4 Summary and concluding remarks

The main conclusions of the research carried out in this project are the following.

1. The acoustic response of an interface formed by rough surfaces in contact has been predicted by theoretical models which recover the macroscopic mechanical properties of such an interface from the statistical properties of the distribution of contacts and from the force laws describing their dynamics. A favourable comparison between the theoretical predictions and the experimental results support the conclusion that *a good understanding of the most important mechanisms intervening in the generation of the higher harmonics by the interface has been achieved.*
2. The magnitude of the nonlinear response predicted by the model and measured experimentally are well above the noise threshold, even for values of the applied pressure of the order of 200 MPa. Amplitude values of the second harmonic which are nearly 40 dB above the noise have been observed on ‘fresh’ rough surfaces. With interfaces having asperities that have been plastically deformed prior to the experiment, the amplitude of the generated second harmonic ranges between 25 and 30 dB above the noise level. Therefore, *we have proved that the dynamic range offered by second harmonic’s generation is quite suitable for detecting and imaging the nonlinear properties of interfaces formed by rough surfaces in contact.*
3. A theoretical model which describes the nonlinear scattering by a two dimensional surface-breaking crack has been developed. It shows that *the experimental configuration yielding the most efficient second harmonic generation is that in which an SV wave insonifies the surface containing the crack at an angle of incidence just above the critical angle for longitudinal waves.* Both linear and nonlinear response are dramatically reduced for values of the angle of incidence around or larger than 45 degrees. This theoretical prediction has been confirmed for an SV wave linearly scattered by a fabricated surface-breaking *defect* and a research proposal to validate this finding on *realistic fabricated cracks* has been submitted to SKI and other organizations for financial support. Finally, as discussed in the report, this configuration, by displaying an increased sensitivity to defects located at or very near the surface of the inspected sample, provides also the way to localize the defect itself. In conclusion, *a full understanding of the mechanisms responsible for the generation and spatial distribution of the nonlinear ultrasonic field has been achieved. Furthermore, the model has provided important information concerning the optimization of the experimental set-up to be used for detecting surface-breaking cracks.*
4. Clear directions for future research and development have emerged from the results discussed above, and will be presented in a proposal under preparation.

5 Acknowledgments

The author wishes to thank SKI for the financial support which has made this investigation possible.

6 References

- Achenbach, J.D., Keer, L.M., Mendelsohn, D.A., *Elastodynamic analysis of an edge crack*, J. Appl. Mech. 47, 551-556, 1980.
- Achenbach, J.D., Norris, A.N., *Loss of specular reflection due to nonlinear crack-face interaction*, J. Non-Destruct. Eval. 3, 229-239, 1982.
- Adler, R. J., and Firman, D., *A non-Gaussian model for random surfaces*, Philos. Trans. R. Soc. London A 303, 433-462, 1981.
- Baik, J.M., and R.B. Thompson, *Ultrasonic scattering from imperfect interfaces: a quasi-static model*, J. Non-Destruct. Eval. 4, 177-196, 1984.
- Baltazar, A., Rokhlin, S.I., and Pecorari, C., *On the relationship between ultrasonic and micro-mechanic properties of contacting rough surfaces*, J. Mech. Phys. of Solids 50, 1397-1416, 2002.
- Bradley, R.S., *The cohesive force between solid surfaces and the surface energy of solids*, Phil. Mag. 13, 853-862, 1932.
- Brown, S. R., and Scholz, C. H., *Closure of random elastic surfaces in contact*, J. Geophys. Res. 90, 5531-5545, 1985.
- Donskoy, D., Sutin, A., and Ekimov, A., *Nonlinear acoustic interaction on contact interfaces and its use for nondestructive testing*, NDT&E International 34, 231-238, 2001.
- Fuller, K.N.G., Tabor, D., *The effect of surface roughness on the adhesion of elastic solids*, Proc. R. Soc. of London, Ser. A 345, 327-342, 1975.
- Goryacheva, I.G., Makhovskaya, Y.Y., *Adhesive interaction of elastic bodies*, J. Appl. Math. and Mech., 65, 273-282, 2001.
- Greenwood, J.A., and Williamson, J.B.P., *Contact of nominally flat surfaces*, Proc. R. Soc. London A 295, 300-319, 1966.
- Greenwood, J.A., Johnson, K.L., *An alternative to the Maugis model of adhesion between elastic spheres*, J. Phys. D: Appl. Phys. 31, 3279-3290, 1998.
- Greenwood, J.A., *Adhesion of elastic spheres*, Proc. R. Soc. London, Ser. A 453, 1277-1297, 1998.
- Guyer, R.A., Johnson, P.A., *Nonlinear mesoscopic elasticity: evidence for a new class of materials*, Physics Today, 4, 30-36, 1999.
- Hirose, S., Achenbach, J.D., *Higher harmonics in the far field due to the dynamic crack-face contacting*, J. Acoust. Soc. Am 93, 142-147, 1993.

Hirose, S., *2-D scattering by a crack with contact boundary conditions*, Wave Motion 19, 37- 49, 1994.

Inagaki, K., Matsuda, O., Wright, O.B., *Hysteresis of the cantilever shift in ultrasonic force microscopy*, Appl. Phys. Lett., 80, 2386-2388, 2002.

Johnson, K.L., Kendall, K., Roberts, A.D., *Surface energy and contact of elastic solids*, Proc. R. Soc. London, Ser. A 324, 301-313, 1971.

Johnson, K.L., *Contact Mechanics*, Cambridge University Press, New York, 1985.

Kim J.-Y., Baltazar A., Rokhlin S.I., *Ultrasonic assessment of rough surface contact between solids from elastoplastic loading-unloading hysteresis cycle*, to appear in the Journal of the Mechanics and Physics of Solids.

Krohn, N., Stoessel, R., Busse, G., *Acoustic non-linearity for defect selective imaging*, Ultrasonics 40, 633-637, 2002.

Maugis, D., *On the contact and adhesion of rough surfaces*, J. Adhesion Sci. and Tech., 10, 161-175, 1996.

Meegan, D.G. Jr., Johnson, P.A., Guyer, R.A., McCall, K.R., *Observations of nonlinear elastic wave behavior in sandstone*, J. Acoust. Soc. of Am., 94, 3387-3391, 1993.

Mendelsohn, D.A., Achenbach, J.D., Keer, L.M., *Scattering of elastic waves by a surface-breaking crack*, Wave Motion 2, 277-292, 1980.

Mindlin, R.D., and Deresiewicz, H., *Elastic spheres in contact under varying oblique forces*, J. Appl. Mech. 20, 327-344, 1953.

Note 1: According to its original definition, μ is the ratio between the extension of the contact at which its rupture occurs under fixed load, $(R\Delta\gamma^2/E'^2)^{1/3}$, and the range of the interaction potential between the surfaces, ε : $\mu = (R\Delta\gamma^2/E'^2)^{1/3}/\varepsilon$. However, for two spheres interacting via a Lennard-Jones force law, $\varepsilon = 1.026\Delta\gamma/\sigma_o$, which renders the definition of μ by Greenwood and Johnson (1998) equivalent to that by Tabor for all practical purposes.

Note 2: The notation $f = f(x|\alpha)$ is used to describe the dependence of the dependent variable f on the independent variable x and on a system parameter α .

O'Neil, B., Maev, R.G., and Severin, F., *Distorsion of shear waves passing through a friction coupled interface*, Rev. Progr. QNDE Vol. 20, Ed. D.O. Thompson and D.E. Chimenti, Am. Inst. of Physics, New York, 1261-1267, 2001.

Ostrovsky, L.A., Johnson, P.A., *Dynamic nonlinear elasticity in geomaterials*, La Rivista del Nuovo Cimento, 24 (7), 1-46, 2001.

- Payzant E.A., Spooner S., Zhu X., Hubbard C. R., *Experimental determination of residual stress by neutron diffraction in a boiling water reactor core shroud*, AMSE NDE Engineering Codes and Standards and Material Characterization, PVP-Vol. 322/NDE-Vol.15, 55-61, 1996.
- Pecorari, C., *Scattering of a Rayleigh wave by a surface-breaking crack with faces in partial contact*, Wave Motion 33, 259-270, 2001.
- Pecorari, C., *Nonlinear interaction of plane ultrasonic waves with an interface between rough surfaces in contact*, J. Acoust. Soc. Am., 113, 3065-3072, 2003.
- Pecorari, C., *Adhesion and nonlinear scattering by rough surfaces in contact: Beyond the phenomenology of the Preisach-Mayergoyz framework*, submitted to JASA (2004a).
- Pecorari C., Poznic M., *Nonlinear scattering by a partially closed surface-breaking crack*, submitted to JASA (2004b).
- Shui, Y., Mao, Y., Jiang, W., Wu, W., and Solodov, I.Y., *The second harmonic generation of bulk acoustic waves reflection*, Proceedings of the IEEE Ultrasonics Symposium, Ed. B.R. McAvoy, IEEE, New York, 429-432, 1987.
- Solodov, I.Y., *Ultrasonics of non-linear contacts: propagation, reflection and NDE applications*, Ultrasonics 36, 383-390, 1998.
- Solodov, I.Y., Krohn, N., and Busse, G., *CAN: an example of non-classical acoustic nonlinearity in solids*, Ultrasonics 40, 621-625, 2002.
- Solodov, I.Y., and Korshak, B.A., *Instability, chaos, and 'memory' in acoustic wave – crack interaction*, Phys. Rev. Lett. 88, 014303, 2002.
- Solodov, I.Y., *Ultrasonics of nonlinear interfaces in solids: new physical aspects and NDE applications*, Proceedings of the 5th Ultrasonics World Conference, 555-564, 2003.
- TenCate, J.A., Van Den Abeele, K.E.-A., Shankland, T.J., *Laboratory study of linear and nonlinear elastic pulse propagation in sandstone*, J. Acoust. Soc. Am. 100, 1383-1391, 1996.
- Van Den Abeele, K.E.-A., Johnson, P.A., Guyer, R.A., McCall, K.R., *On the quasi-analytic treatment of hysteretic nonlinear response in elastic wave propagation*, J. Acoust. Soc. Am., 101, 1885-1898, 1997.
- Van Den Abeele, K.E.-A., Carmeliet, J., Johnson, P.A., Zinszner, B., *Influence of water saturation on the nonlinear mesoscopic response of earth materials, and the implications to the mechanism of nonlinearity*, J. of Geophys. Res., 107, 101029-101040, 2002.
- ZaisteV, V.Y., Gusev, V., and Castagnede, B., *Observation of the 'Luxenburg-Gorky' effect for elastic waves*, Ultrasonics 40, 627-631, 2002.

ZaisteV, V.Y., Gusev, V., and Castagnede, B., *Luxenburg-Gorky effect retooled for elastic waves: a mechanism and experimental evidence*, Phys. Rev. Lett. 89, 105502, 2003

www.ski.se

STATENS KÄRNKRAFTINSPEKTION
Swedish Nuclear Power Inspectorate

POST/POSTAL ADDRESS SE-106 58 Stockholm

BESÖK/OFFICE Klarabergsviadukten 90

TELEFON/TELEPHONE +46 (0)8 698 84 00

TELEFAX +46 (0)8 661 90 86

E-POST/E-MAIL ski@ski.se

WEBBPLATS/WEB SITE www.ski.se